LOCALIZATION OF QUANTUM WALKS ON TREES WITH DISORDER

by

STEVEN JACKSON

Frederick W. Strauch, Advisor

A thesis submitted in partial fulfillment
of the requirements for the
Degree of Bachelor of Arts with Honors
in Physics

WILLIAMS COLLEGE

Williamstown, Massachusetts

May 19$^{\text{th}}$, 2010

Acknowledgements

Like any work of science, this thesis was made possible by the support of many whose names don't appear on the title page. Foremost among these are my parents, Tom and Bonnie, who did a wonderful job of fostering and supporting my interest in science and academics from an early age and have always encouraged me to pursue my interests.

The faculty and staff of the Physics department have also provided a fantastic education and valued guidance whenever needed. The colloquia have provided a wonderful opportunity to hear about new and exciting areas of physics that aren't necessarily standard parts of the undergraduate curriculum, and the snacks afterwards were never to be missed!

I'd also like to thank all of my friends at Williams, especially those in the Physics department and those on the Cross Country team, who have all been incredibly supportive and made my time at Williams all the more enjoyable.

Though he has not been directly involved in this research, Prof. Steve Miller has also helped influence this project through my work with him in SMALL 2009, which introduced me to Random Matrix Theory and many other mathematical techniques applicable to physics.

I am also indebted to Prof. David Tucker-Smith, who has provided helpful comments as my second reader, especially for identifying specific changes that could clarify certain ideas for people who haven't worked on these topics for a year.

Finally, I am very appreciative of the support provided by my advisor Prof. Fred Strauch throughout the creation of this thesis. The help he has provided throughout the writing of this thesis has proved to be invaluable, whether in making sure I was progressing adequately throughout the first semester, improving or debugging my programs, discussing physics or mathematics related to the thesis, or making suggestions to improve my writing. Without his guidance this thesis would be significantly diminished in all qualities, and any mistakes remaining are my own.

Executive Summary

Anderson Localization, the phenomenon in disordered systems where there is a transition from extended to localized quantum states, has many important consequences in condensed matter physics. Perhaps most importantly, long-scale transport of particles will cease in systems exhibiting Anderson Localization. For this reason the localization transition is often referred to as a metal-insulator transition, as the disorder disrupts the transport of electrons and current can no longer flow.

Another important development in condensed matter is the possibility of building quantum computers that can perform specific tasks exponentially faster than classical computers. Notably, Childs et al. showed that a quantum walk on a glued trees graph could complete a specific task in only polynomial time, whereas the best possible classical result finishes in exponential time.

However, Childs assumed that there was no disorder in the graph. In reality, any realization of such a graph will not be free from imperfections. There will be couplings to the environment, causing decoherence, and disorder in the Hamiltonian caused by different connection strengths in the edges (off-diagonal disorder) or diagonal disorder in the on-site energies of the nodes of the graph. In this thesis we will consider how diagonal disorder in the Hamiltonian affects the transport properties of particles on these graphs, with an eye toward the disorder's effect on the speedup in the quantum algorithm.

A commonly used Hamiltonian for a graph is the Anderson tight-binding Hamiltonian:

$$\mathcal{H} = \sum_j \varepsilon_j a_j^\dagger a_j - \sum_{\substack{\text{neighbors} \\ i,j}} V_{ij} a_j^\dagger a_i, \tag{1}$$

where $a_j^\dagger$ and a_j are the creation and annihilation operators, respectively, for a particle on node j of the graph. The coefficients ε_j represent on-site energy, whereas V_{ij} represent different connection strengths of edges. In particular, because of our assumption of diagonal disorder, we will consider such Hamiltonians where V_{ij} is always 1 if the nodes are connected, and the ε_j are chosen uniformly in the interval $[-W/2, W/2]$, or equivalently are uniformly distributed with mean zero and width W. We will try to identify the critical disorder, W_C, the minimum value of W for which all eigenfunctions of the Hamiltonian are localized. Our study of the effect of disorder on this graph breaks down broadly into three areas: eigenfunction statistics, spectral statistics, and transport properties of these trees.

Our first measure of localization, the eigenfunction statistics, uses a standard quantity called the inverse participation ratio (IPR). The IPR is defined by the equation

$$\text{IPR} = \sum_j |\psi_j|^4, \tag{2}$$

where ψ_j is the amplitude of the wavefunction at node j. This quantity will be between 0 and 1, with 0 corresponding to an extended state and 1 corresponding to an extremely localized state, since the IPR corresponds to the inverse of the weighted number of nodes on which the wavefunction is nonzero. In order to extract relevant information about the IPR we construct a Hamiltonian for many levels of disorder, calculate the eigenfunctions and the corresponding eigenvalues, then calculate the corresponding IPR while binning over eigenvalues within a small range. For more representative results, we average over many instances of the random Hamiltonian. The results of this graph can be seen in Figure 1. Our numerical results for finite graphs are in qualitative agreement with the predictions of Anderson localization on an infinite Cayley tree, with the critical disorder near 17.

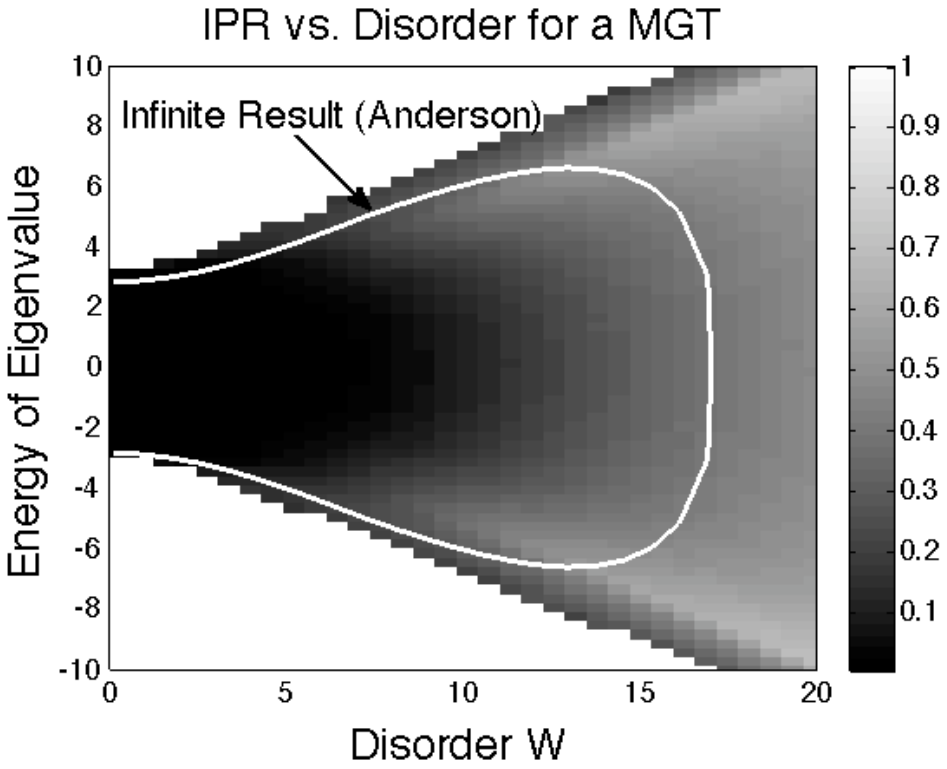

Figure 1: The IPR of the eigenfunctions of the Anderson tight-binding Hamiltonian, indicated by the color of the plot, is plotted as a function of the disorder W and the corresponding energy eigenvalues. For small disorder, the states have a low IPR (extended), while for large disorder the states have an IPR approaching one (localized).

Our second measure, the spectral statistics of the Hamiltonian, is also indicative of the localization transition. Once the spacing s between adjacent eigenvalues is normalized to have mean 1, we calculate the distribution of the nearest-neighbor level spacings $P(s)$. At the critical level of disorder, this distribution should be independent

of the depth of the graph since the critical disorder is a scale free parameter. From standard random matrix theory, it is predicted that this distribution shifts from the Wigner surmise distribution, $P_W(s)$, to the Poisson distribution, $P_P(s)$, as disorder is increased. Since these curves (and all intermediate curves) intersect near $s = 2$, we use the parameter

$$\gamma = \frac{\int_2^\infty P(s) - \int_2^\infty P_W(s)}{\int_2^\infty P_P(s) - \int_2^\infty P_W(s)} \tag{3}$$

to identify the critical disorder by plotting γ versus the disorder for multiple graph depths and identifying the point where all of these curves intersect. This measure suggests that the critical disorder for this graph is between 10 and 11, which is roughly in line with, but lower than, the value estimated from the IPR results.

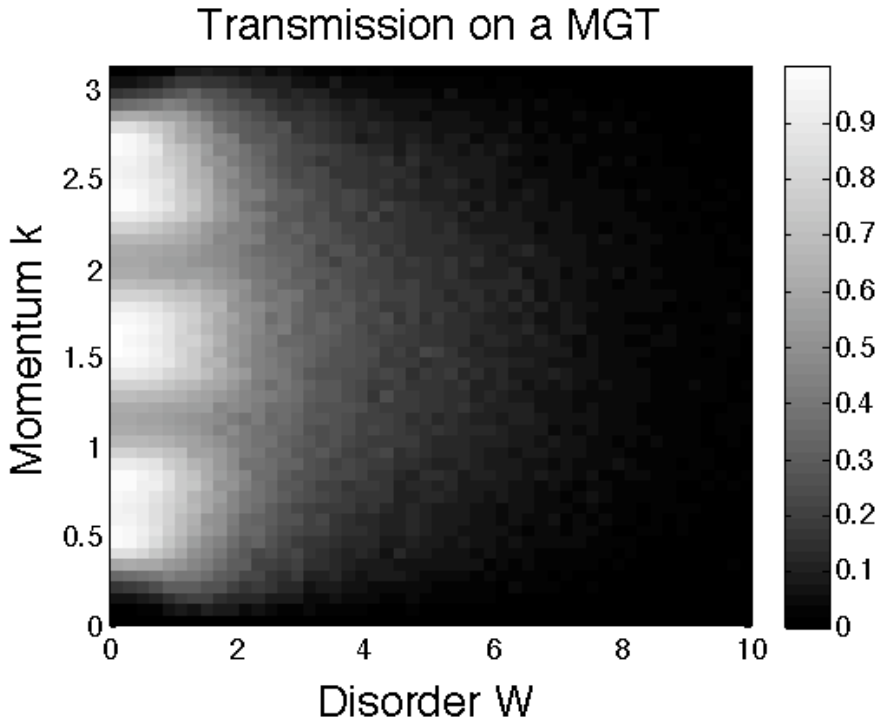

Figure 2: The Transmission of the graph, indicated by the color of the plot, is plotted as a function of the disorder W and the momentum of the incoming particles.

Finally, we consider the transport properties of the graph. We do this by attaching leads to the entrance node and exit node of the graph, sending a wave in, which then produces a reflected wave and a transmitted wave. Requiring this state to be an eigenfunction, we get a set of equations that allows us to perform a formal matrix inversion, which then allows us to calculate the transmission coefficient of the graph. This calculation was performed for graphs of different depths, to see how the transport

scaled with the depth of the tree, and also for different momenta of the incoming wave for a single depth. A representative plot of this calculation is shown in Figure 2. While there are no clear features with which we can identify W_C (and indeed, the plot may not even extend far enough in W), there are many interesting features in this and other similar plots. First is appearance of features at zero disorder, similar to resonances in a Fabry-Perot interferometer, since at $W = 0$ the graph can be collapsed down to a line. Increasing the disorder smooths out these features as the transmission decays. The transmission decays more slowly than expected, and surprisingly appears not to depend on the size of the graph.

While more research is needed to determine how the time it takes for the particle to traverse the graph increases with both disorder and the size of the graph, we have demonstrated that finite instances of the glued trees graph introduced by Childs et al. undergo a localization transition in agreement with previous studies of the (finite and infinite) Cayley tree. We have also introduced a new method to calculate transmission through such graphs. Our results suggest that quantum walks with disorder less than the critical disorder could still be a useful primitive in quantum computation.

Contents

Chapter 1

Introduction

Anderson Localization has a rich history, from P.W. Anderson's original paper in 1958 to more recent research, ranging from numerical simulations of localization [MD], analysis using supersymmetric methods [MF] to mathematical proofs of the existence of non-localized states in certain systems [Klein]. Many systems of sufficiently high dimension support extended quantum states that are uniformly distributed throughout the system. These extended states are critical for quantum transport of particles, such as an electron in a crystal. However, beyond some critical level of disorder, all wavefunctions will become localized, and transport will cease. This is the essence of the localization transition. This transition is also described as a metal-insulator transition because of the effects on electron transport. While there are certain systems in which the localization transition has been quite well studied and characterized, there are still many systems of importance for which it is less well understood.

The root cause of Anderson Localization is quantum interference between the possible paths from one location to another. If the interference tends to be strongly destructive, then we have Anderson Localization, in which the amplitude of the particle is exponentially suppressed beyond the localization length. Of course, the greater the number of possible paths, the harder the calculation will be, so the best understood systems tend to be those in which there are relatively few possible interactions between paths. Among these are the one-dimensional case, in which localization has been shown to be inevitable with any disorder by Slevin and Pendry [SP], and the Cayley tree, a system quite similar to those we'll be studying throughout this paper and solved by Abou-Chacra et al. in [ACAT]. The *Cayley tree* is a graph with no loops in which every node has the same number of neighbors. This makes the Cayley tree especially easy to study since there is only one direct way to make it from a given node to any other, and so although it behaves emphatically unlike a one-dimensional system, many aspects of the analysis simplify in a similar manner.

Another important field in physics is that of quantum computation, which has blossomed in recent years. What makes quantum computation so powerful is that certain problems that are intractably difficult to solve classically can be solved much

more quickly using applications of quantum mechanics. Probably the most famous of these is Shor's algorithm, which finds the prime factors of an integer exponentially faster than the best known classical algorithm, which would thus have a large impact on the RSA encryption that is currently widely used for electronic transactions, particularly on the internet. A great amount of theoretical work in quantum computing is thus directed towards finding other quantum algorithms that perform exponentially faster than the best classical counterparts.

One candidate for exponential speedup is the quantum walk, which behaves quite differently from a classical walk. In particular, the behavior that makes it a likely candidate is that quantum walks tend to move much faster — for a quantum walk the expectation value of the distance squared scales as $\langle x^2 \rangle \propto t^2$, whereas for a classical walk it scales like $\langle x^2 \rangle \propto t$, where t is the number of time steps taken. Quantum walks will be discussed more fully in section 2.1.

As was demonstrated by Childs et al. [CCF+], a search on somewhat modified binary glued trees (see 1.2(b)) can be done exponentially faster with a quantum walk than a classical random walk. This system is the one we will focus on, but we will postpone the details of their results until after we have introduced the graphs in question.

Experimentally, much of the focus is on producing systems that behave like the idealized systems considered by theorists. Thus, experimentalists have to worry about effects like quantum decoherence due to couplings between the system and the environment, producing systems that behave like idealized quantum bits (qubits), and disorder in the system due to possible flaws in the manufacturing process, which can include differing connection strengths between qubits or different on-site energies for different qubits. Recent experimental results can be found in the papers by Karski et al. [KFC+], Zahringer et al. [ZKG+], and Broome et al. [BFL+].

However, Childs assumed that the tree had no disorder, but any quantum walk implemented in nature is likely to have those imperfections encountered by experimentalists. While we won't address the problem of decoherence, this paper seeks to address the question of how disorder on a glued tree affects the transport of a quantum walk, and in turn how that affects the speedup of the quantum walk over the classical one. Using other methods to analyze this problem, Keating et al. found that the localization length, which is roughly the length of area a particle can expect to travel, decreases with increasing disorder [KLMW].

1.1 Graphs and a Forest of Trees

Since our discussion of localization will be limited to graphs, we begin by introducing some graph terminology, then the specific graphs that this paper will focus on, as well as the Hamiltonian we will use for these graphs. A graph can be thought of as a set of *nodes* or *vertices* (which we will use interchangeably), along with a set of undirected *edges* that connect these nodes. For our purposes, at most one edge will directly

connect any two nodes (though longer paths through multiple edges are of course possible) and no node can have an edge that returns to itself, except in one specific case. A *leaf node* is a node that has only one edge. The *degree of a node* is simply the number of edges connected to that node. That is, a node will be of degree n if it connects to n other vertices. A graph in which every node is of degree n is called an *n-regular graph*. Most of the graphs we'll work with will be nearly 3-regular, but they will contain some nodes of degree 1 or 2 as well. A *Cayley tree* is an n-regular graph that has no loops. Next, a *planar graph* is one that can be represented in a plane with no edges crossing each other. Clearly, it is much easier to construct a physical representation of a planar graph than a non-planar graph, as in planar graphs one won't have to worry about wires having to cross large distances, thus affecting the connection strength between those nodes, or by crossing and interfering with other wires. Finally, the *adjacency matrix* A of a graph is simply a matrix representation of how its nodes are connected to each other, with its entries a_{ij} satisfying

$$a_{ij} = \begin{cases} 1 & \text{there is an edge between nodes } i \text{ and } j, \\ 0 & \text{there is no edge between nodes } i \text{ and } j. \end{cases} \tag{1.1}$$

For example, for the simple graph of a square, with the nodes being the corners of the square, we see that

$$A = \begin{pmatrix} 0 & 1 & 1 & 0 \\ 1 & 0 & 0 & 1 \\ 1 & 0 & 0 & 1 \\ 0 & 1 & 1 & 0 \end{pmatrix} \tag{1.2}$$

will be its adjacency matrix. Since the edges are undirected, the adjacency matrix of a graph will be real, symmetric, and with real eigenvalues.

We now introduce the various trees, describe how to construct them, and provide images of smaller examples. The effect of disorder on the infinite limit of the Simple Branched Tree has been solved, but the effect on the other graphs has, to our knowledge, not been completely characterized as of yet.

1.1.1 Simple Branched Tree (SBT)

We begin by considering binary branched trees. An example of a small simple branched tree is shown in Figure 1.1(a). In these trees the graph ends after $d-1$ branchings, and all nodes except for the leaf nodes have precisely two child nodes. A depth d branched tree will have $2^{d+1}-1$ vertices, and since each non-leaf node has two children this tree must also have $2(2^d-1)$ edges. For computational purposes we number the nodes by labeling the leftmost node in the graph as node 1, then numbering consecutively while proceeding downwards through each column, moving a column to the right once the current column ends. With this numbering system, we then have that vertex k is connected to vertex $2k$ and vertex $2k+1$, provided that $k < 2^{d-1}$.

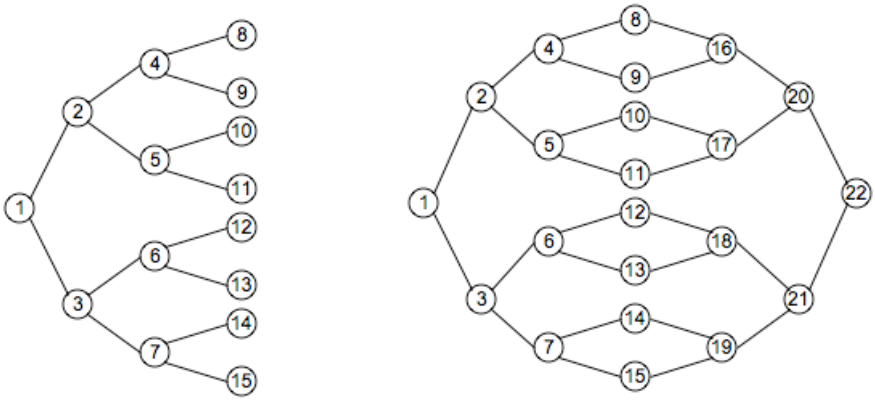

(a) (b)

Figure 1.1: **(a):** S depth 3 simple branched tree. Note how the leaf nodes 8 through 15 are all of degree one, rather than degree three. **(b):** A depth 3 simple glued tree. The central column consisting of nodes 8 through 15 are of degree two, hence a large fraction of the nodes fail to preserve the local structure of the Cayley tree.

We note that the simple structure of these branched trees means that the leaves of the graph have degree one, whereas all other vertices except the first have degree three. Thus, the local structure of the tree is not preserved at the leaves, and as they constitute roughly half of the vertices of the tree, this can lead to anomalous effects on the eigenfunctions of the graph in the presence of disorder.

While this may superficially appear to become a Cayley tree in the limit $d \to \infty$, we shall see that this is not actually true. The difference is due to the fact that any instance of a simple branched tree will have roughly half of its nodes be leaf nodes, whereas the Cayley tree has no leaf nodes, so there is no reason to expect similar behavior. As we shall see, these leaf nodes can lead the simple branched trees to have behavior quite unlike that of the Cayley tree.

1.1.2 Simple Glued Tree (SGT)

One way to modify the branched tree — and first introduced to quantum walks in [CCF+] — is by "gluing" two branched trees together. Such a graph is shown in Figure 1.1(b). We now describe the structure of these trees.

For glued trees, the structure begins with a binary branching tree of depth d on the left, oriented so that it opens to the right, a column of 2^d vertices in the middle, then another binary branching on the right that opens to the left. Thus, by summing the number of vertices in the two trees with the central column, we have $N = 3 \cdot 2^d - 2$ vertices on a glued tree of depth d. One can also calculate that, since there are $2 \cdot 2^d - 2$ nodes (that is, all non-central nodes) each with two children, there must be $4(2^d - 1)$

edges in a simple glued tree graph.

We number the vertices as for the branched tree, then connect the first branched tree exactly as in the manner described above. For the other branched tree, we connect it in the same manner but proceeding backwards from the last vertex, so for example vertex $N+1-k$ is connected to vertices $N+1-2k$ and $N+1-(2k+1)$, where $N = 3 \cdot 2^d - 2$.

Although it is not quite as obvious as in the simple branched trees, there are still a large number of vertices lacking the local structure of the infinite Cayley tree. In fact, all of the vertices in the central column, which constitutes roughly a third of the vertices in the graph, are of degree two rather than degree three. Again, we shall see that this leads to anomalous effects when we study the localization transition.

1.1.3 Modified Branched Tree (MBT)

We will now consider a modification of the branched tree that preserves the local structure at the leaves, as pictured in 1.2(a). In order to perform this modification, we can randomly connect each leaf vertex to exactly two others. We first note that this adds no new nodes, but does add a total of 2^{d-1} edges, since we need to avoid double-counting the two edges that are added to each of 2^{d-1} leaf nodes. Thus, the total number of edges is now $3 \cdot 2^{d-1} - 2$. This was implemented computationally by generating a random permutation of the positive integers through 2^{d-1}, then connecting vertex $k + 2^{d-1} - 1$ to the $(k-1)^{\text{th}}$ and k^{th} (modulo 2^{d-1}) elements of this permutation. In order for these numbers to correspond to leaf vertices, we must of course add $2^{d-1} - 1$ to these elements of the permutation. As described, this doesn't preclude a vertex from connecting to itself, but as we are averaging over many instances of these graphs and the expected number of self-connections is low, this flaw should not significantly affect our results. Finally, we note that most representations of the modified branched tree will not be planar graphs, thus making it more difficult to implement in a physical system.

1.1.4 Modified Glued Tree (MGT)

To make a modified glued tree, we must make somewhat more substantial changes to the glued tree, as seen in Figure 1.2(b). We now will have two central columns of 2^d vertices, for a total of $4 \cdot 2^d - 2$ vertices in the graph (that is, two simple branched trees of depth $d+1$ facing each other). We now connect the two central columns together so that each vertex is connected to exactly three others (including their preexisting connections within the branched tree). The number of edges on this graph will be the sum of two SBTs of depth $d+1$ plus the number of edges added, or $6 \cdot 2^d - 4$.

Our procedure to implement this computationally is similar to that for the modified branched tree. We generate a random permutation of the positive integers through 2^d, then use this to connect the vertices as follows. Vertex $k + 2^d - 1$

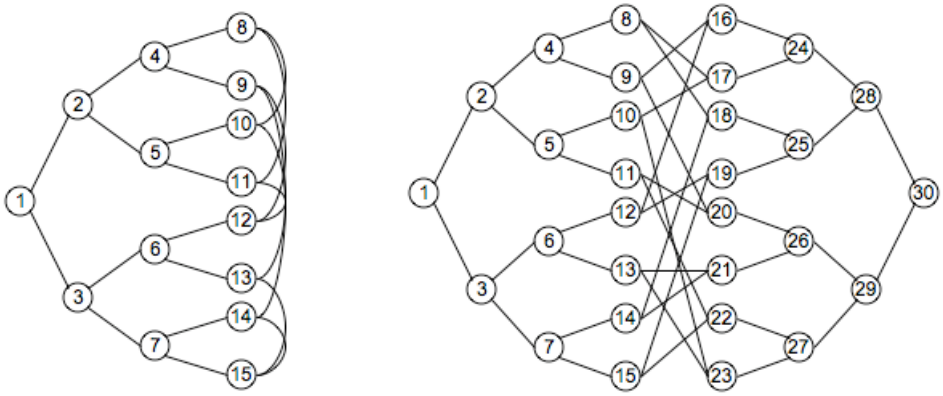

(a) (b)

Figure 1.2: **(a):** A representation of a depth 3 modified branched tree. The modifications change the structure of the graph so that it no longer includes leaf nodes. **(b):** A representation of a depth 3 modified glued tree. In this case, the modifications add a new central column of nodes and connect the two columns so that all central nodes are of degree three.

will be connected to the vertices corresponding to the $(k-1)^{\text{th}}$ and k^{th} elements of this permutation. As with the modified branched tree, we add $2^{d+1}-1$ to these elements to get the corresponding vertices. For these graphs there is no possibility of self-connections like we had with the modified branched tree.

It is also important to note that for both of the modified trees we might expect behavior more like that of the Cayley tree since for any depth (almost) every node is of degree three. However, the method of construction of these graphs also creates many loops, which might alter the effects of disorder in some other way.

Finally, note that the two modified trees are no longer planar graphs. One might suppose that these would have limited physical significance. However, the modified glued tree is the system where Childs et al. [CCF+] found the exponential speedup in the quantum walk over the best classical algorithm. In addition, superconducting circuits are being explored with many non-planar structures, as in Strauch and Williams [SW] and Helmer et al. [HMF+]. Thus, despite the fact that the modified glued tree is non-planar, this is the most important of the graphs that we will study.

1.2 Previous Results

For all of these trees, we will describe the Hamiltonian of this system using the Anderson tight-binding model, which was original motivated by disordered potentials and electrons on a lattice. It can also be used to describe coupled spin (quantum bit,

or qubit for short) systems [Bose], and exciton dynamics in photosynthetic molecules [RMKLA]. It takes the form

$$\mathcal{H} = \sum_j \varepsilon_j a_j^\dagger a_j - \sum_{\substack{\text{neighbors} \\ i,j}} V_{ij} a_j^\dagger a_i, \tag{1.3}$$

where $a_j^\dagger$ and a_j are the creation and annihilation operators, respectively, for a particle to be on the node j, and V_{ij} is a matrix representing possible off-diagonal disorder. Here the question arises of whether the disordered on-site energies ε_j or disordered off-diagonal couplings V_{ij} are most significant. It turns out that for superconducting circuits the disordered couplings are most conducive to localization. However, since most of the existing research has focused on diagonal disorder, which has proved to be an interesting problem, we will follow their lead and assume that $V_{ij} = 1$ for all neighbors i and j. Thus, the latter term simply becomes the adjacency matrix of this graph, while the first term represents the on-site, or diagonal, disorder of the graph. For the remainder of the paper, we will consider, for a level of disorder W, ε_j to be uniformly distributed on an interval of width W centered at zero: $[-W/2, W/2]$.

This hamiltonian can then be inserted into the Schrodinger equation

$$\frac{d}{dt}|\psi(t)\rangle = \mathcal{H}|\psi(t)\rangle, \tag{1.4}$$

which can then be solved to yield

$$|\psi(t)\rangle = e^{-i\mathcal{H}t}|\psi(0\rangle, \tag{1.5}$$

which can be solved for in terms of the spectral properties of $\mathcal{H}$.

The Anderson tight-binding model has previously been used to study the infinite limit of a branched tree, called a Cayley tree or a Bethe lattice, and this case has been solved analytically by Abou-Chacra et al. in [ACAT] and [ACT]. By imposing the Anderson tight-binding Hamiltonian on a graph, they defined a quantity called the self-energy in relation to the Green's function for the system. Following the results that could be inferred by applying the self-energy for this system, they obtained an equation defining the distribution of the self-energy in terms of itself. By demanding that this distribution was self-consistent, they were then able to characterize localization by whether or not the imaginary parts of the distribution persists under certain conditions. Using equations (5.4) and (5.5) from [ACT], one can determine the critical disorder for Cayley trees, which turns out to be around 17 for a degree 3 Cayley tree. Thus, we can hope to learn about the localization transition on glued trees through comparison to the branched tree graph, and much of the paper is focused on exploring what similarities and differences these graphs exhibit.

These same equations also allow one to calculate the location of the *mobility edge* which separates the localized states and extended states, as seen in Figure 1.3 based on their calculations. This is defined by calculating, for each value of W,

the critical energy E_C above which (in absolute value) all states are localized. The critical disorder W_C is then defined as the level of W at which E_C drops to zero, or equivalently as the level of W above which there are no extended states.

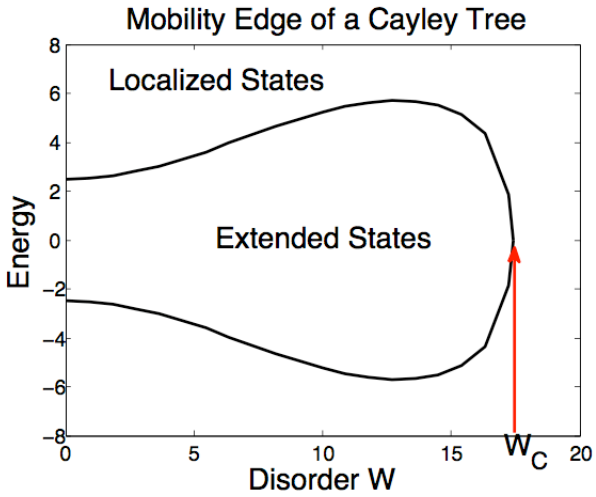

Figure 1.3: A plot of the mobility edge, which separates extended states in the interior curve from localized states in the exterior, for a Cayley tree with degree 3. The critical disorder W_C is the level above which there are no extended states.

The remaining structure of the paper is as follows. In Chapter 2, we introduce the methods and definitions integral to our study, including a more in-depth discussion of quantum walks and the other methods we'll use to analyze the localization transition. We then present the results of our different methods of analysis. In Chapter 3 we look at localization through a characterization of wavefunctions, in particular the eigenfunctions of the Hamiltonian. Next, we observe the effects of disorder on the spectral statistics of the Hamiltonian in Chapter 4, and use the scale-independence of the localization transition to hone in on the critical disorder. Our final method is calculating the transmission coefficient of an incident wave on the graphs, and observing how it scales with both the disorder and the size of the graph. Through these explorations, we discover that we need to modify our graphs to get the desired behavior, and henceforth focus on these modified graphs. We also note that the behavior of the modified glued tree graph closely mimics that of the modified branched tree, on which localization is better understood. Finally, we end with a discussion of the results and possible directions for future research in Chapter 6.

Chapter 2

Methods and Definitions

In this chapter, we give a brief summary of the important methods and definitions that we will use to study the localization problem on graphs. In addition, we give a more fully fleshed out discussion of quantum walks, given its importance in the algorithm of Childs et al. Moreover, Childs has recently shown in [Chi] that quantum walks on graphs can perform universal computation with a Hamiltonian consisting of only the adjacency matrix of the graph. Thus, quantum walks are an important component of the field of quantum computation.

2.1 Quantum Walks

We now give a more formal discussion of quantum walks vs. classical walks on graphs, beginning with a quick review of classical walks.

A classical random walk, often likened to a drunkard's walk, on a graph is determined by a "coin flip" of sorts, with each path available being equally likely to be chosen. Thus, for a classical random walk on a line, where there are only two choices, for which path to take, one can calculate that $\langle x^2 \rangle = t$, where t is the number of steps taken.

Of course, we aren't just comparing a quantum walk to a classical random walk, but instead to the best possible classical algorithm. In many systems, a classical walker could use local information and markings to improve upon a random walk and reach their destination much faster, as most (sober) human walkers do. However, in certain systems, such as the modified glued trees in [CCF+], the local information is the same at each node and markings don't help in any significant manner, hence the classical random walk is a near optimal strategy.

On the other hand, a quantum walk (QW) can be quite different. For one thing, a quantum walk can either be a discrete time QW, where the walk is governed by a coin operator, or a continuous time QW [Kempe], which is typically governed by the

adjacency matrix Hamiltonian[1], and follows the usual evolution rule

$$|\psi(t)\rangle = e^{-i\mathcal{H}t}|\psi(0)\rangle. \tag{2.1}$$

Both of these quantum walks can exhibit the same type of speedup over the classical random walk, though the discrete time QW is of course sensitive to the choice of the coin operator, whereas the continuous time QW only depends on the specifics of the adjacency matrix. However, both the discrete time QW (for appropriately chosen coin operators), and the continuous time QW will have $\langle x^2\rangle \propto t^2$, and so rather than slowly diffusing throughout system it will steadily move outwards from its starting location.

For an ordered glued tree, we can further simplify the analysis of a continuous time quantum walk by noting that what the wavefunction does at each node of a certain depth is independent of which node we look at, so that we can project into the *column space* of the graph. This discussion of the column space closely follows that of Childs et al. Column-space wavefunctions are simply even superpositions of each node in the column, normalized to have probability 1. Referring back to Figure 1.2(b), for example, we have

$$|\text{col } 3\rangle = \frac{1}{\sqrt{8}}\sum_{j=8}^{15}|j\rangle. \tag{2.2}$$

More generally, for a MGT of depth d, numbering the columns from 0 to $2d+1$ we consider the $(2d+2)$ states defined as follows:

$$|\text{col } j\rangle = \frac{1}{\sqrt{N_j}}\sum_{a\in\text{column } j}|a\rangle, \tag{2.3}$$

where N_j is the number of nodes in column j, so that

$$N_j = \begin{cases} 2^j & 0 \le j \le d, \\ 2^{2d+1-j} & d+1 \le j \le 2d+1. \end{cases} \tag{2.4}$$

This reduces the problem to a quantum walk on a line in which not every connection is of strength one. In order to define the column space Hamiltonian, we note that in the first half of the graph there are two connections from each node in column j to a node in column $j+1$, but that each node in column $j+1$ has a weighting of $1/\sqrt{2}$ that of a node in column j. Thus, $\langle \text{col } j|\mathcal{H}|\text{col } (j+1)\rangle = \sqrt{2}$ in this case. Similarly, the first central column has 2 connections for each node to the next and the same

[1]The Laplacian of the graph can also be used, which is the adjacency matrix plus diagonal elements equal to the negative of the degree of the node. This can lead to different characteristics in the quantum walk, but for the MGTs of interest all but two nodes are of degree three, so this reformulation has little effect beyond redefining zero energy.

weighting for each node, and the rest of the entries are determined by symmetry, so we have the general formula for the Hamiltonian:

$$\langle \text{col } j|\mathcal{H}|\text{col } (j+1)\rangle = \begin{cases} \sqrt{2} & j \neq d, \\ 2 & j = d. \end{cases} \tag{2.5}$$

This reformulation of the quantum walk on a graph with no disorder greatly simplifies many aspects of the calculations, and also allows for a simple calculation of the transmission of such a graph, as we'll perform later.

Now that we have a firmer grasp of the intricacies of quantum walks, we return to the results of [CCF+]. They considered the case where the walker is trying to reach the rightmost node, henceforth END, on a simple branched tree from the leftmost node, henceforth START. Since this graph always has two paths towards the center of the graph, and only one path away from the center, a classical random walk will tend to get stuck in the center of the graph and will require an extremely fortuitous string of choices to reach the rightmost node. On the other hand, the quantum walk can split coherently between the possible paths, hence some part of the wavefunction will reach the rightmost node in linear time.

However, as noted above, a classical random walk isn't always the most effective way to find your way to the goal. As it turns out, the simple glued tree provides local information for the classical walker that he can use so that the quantum walk doesn't have an exponential speedup. The first time he reaches a node of degree 2, he knows that he's at the middle of the graph and on the right track, and continues on his way. The next time he reaches a node of degree two, he'll know that he's heading the wrong way and can backtrack. In this way, he can improve greatly on the classical random walk and reach END much faster.

If we now replace the simple glued tree with a modified glued tree, the classical walker no longer has any access to useful local information, and thus can't improve on the random walk in any meaningful way. Moreover, this new structure proves to have no effect on the quantum walk, so it can reach END in the same time as before, and thus achieve the exponential speedup over the classical walk.

2.2 Inverse Participation Ratio

In order to characterize the localization transition on our graphs based on the eigenfunctions of the Hamiltonian, we need some measure of how localized a wavefunction is. The inverse participation ratio (IPR) is just that — a simple way to summarize how extended or localized a given wavefunction is. The IPR of a wavefunction on a graph is defined by the sum over all nodes of the fourth power of the absolute value of the wavefunction at that node:

$$I = \sum_j |\psi_j|^4. \tag{2.6}$$

This is called the *inverse* participation ratio because it is essentially the inverse of the number of sites (when appropriately weighted) where the wavefunction is non-zero. For example, if a wavefunction is evenly spread over N sites, from the normalization of the wavefunction we know that $|\psi_j|^2 = 1/N$ for each j, hence

$$I = \sum_j |\psi_j|^4 = \sum_j \left(\frac{1}{N}\right)^2 = \frac{1}{N}, \tag{2.7}$$

showing that the IPR indeed behaves as described.

In order to apply this concept to our graphs, we'll consider the IPR of the eigenvectors of the Hamiltonian in equation (1.3), for various values of the disorder. Doing this won't allow us to directly calculate the critical disorder, but will provide some insight to the shape of the mobility edge.

In order to more accurately identify the critical disorder, we can adopt a different procedure. As noted before, the localization transition, and thus the critical disorder, should be scale independent. Thus, as argued in [BST], beyond the mobility edge the IPR should be independent of the size of the graph. We can therefore locate the critical disorder more precisely by plotting the IPR as a function of the disorder for an eigenvector at the band center for trees of various depths and seeing where the curves first merge.

2.3 Random Matrix Theory

Random matrix theory (RMT) has a rich history in physics, and has been especially useful in areas that are much too complicated to be studied using traditional methods. They were first used to predict the energy levels and level spacings of heavy nuclei like that of Uranium [FM], since the number of bodies and complexity of the interactions make it impossible to determine the Hamiltonian, much less the distribution of its eigenvalues.

Thus, instead of trying to calculate these quantities directly, Eugene Wigner decided to attempt to analyze them using a statistical argument. One can study the eigenvalues of an ensemble of $N \times N$ matrices of the right symmetry class, but with the elements chosen randomly from a given probability distribution, then take the limit $N \to \infty$. As it often turns out, the eigenvalue statistics of such randomly generated matrices will tend toward the ensemble average with probability equal to 1 as $N \to \infty$. Moreover, this ensemble average has provided useful physical predictions, though they are of course statistical, rather than deterministic, in nature.

Of course, our approach being more computational, we won't be able to create and diagonalize infinite dimensional matrices. However, even at finite sizes, there is often a good convergence to the limit of the ensemble average, especially when averaging over multiple instances of these finite matrices [MTB]. Thus, while our results based

on RMT certainly can't be taken to be exact, they will most certainly be reliable approximations of the true answer.

Also, we should note that the symmetry classes of matrices that can be effectively studied are usually limited to those whose eigenvalues can be ordered. Thus, RMT usually focuses on the study of unitary matrices, which although they have complex eigenvalues, all have modulus 1, and thus can be ordered by the principle value of their angle in the complex plane, or Hermitian matrices, which have real eigenvalues and are thus easily ordered. This ordering allows us to study not just the distribution of the eigenvalues, but also allows the definition of adjacent eigenvalues, and thus the distance between adjacent eigenvalues.

One of the most useful RMT results is that for the nearest neighbor spacing distribution of the eigenvalues of large random matrices. The nearest neighbor spacing distribution $p(s)$ is defined by considering the spacing between adjacent eigenvalues, and then normalizing:

$$s = \frac{E_{i+1} - E_i}{\langle E_{i+1} - E_i \rangle}. \tag{2.8}$$

The distribution $p(s)$ is then found by taking the ensemble average of the distribution of s for each matrix.

The most pertinent result for us is the transition in the normalized nearest neighbor spacing distribution that occurs as diagonal disorder is increased. When the diagonal disorder is very large, we can simply treat the matrix as a diagonal matrix, hence the eigenvalue spacing distribution will simply follow the spacing of the distribution that the disorder is chosen from. Since we are choosing the diagonal elements from a uniform distribution, the nearest neighbor spacing distribution will then follow that of N points chosen uniformly, which when normalized to have a mean of 1 will of course follow the standard Poisson distribution:

$$P_P(s) = e^{-s}. \tag{2.9}$$

When the disorder is zero it is less obvious what the spacing distribution will be, but it can be worked out to follow the Wigner surmise distribution [MTB]:

$$P_W(s) = \frac{\pi}{2} s \exp\left(-\frac{\pi}{4} s^2\right). \tag{2.10}$$

Unlike the Poisson distribution, the Wigner surmise distribution exhibits some level of repulsion between neighboring eigenvalues since the distribution is linear in s near the origin. This repulsion can be seen in Figure 2.1, in contrast to the Poisson distribution.

Thus, as the disorder is increased we expect a transition from the Wigner surmise distribution to the Poisson distribution. Moreover, since the critical disorder is a scale-free parameter, we expect that at the critical disorder there is some critical distribution $P_C(s)$ that would be shared by all trees of that type, regardless of size. Thus, if we plot the level spacing distribution for trees of different depths, we'll be

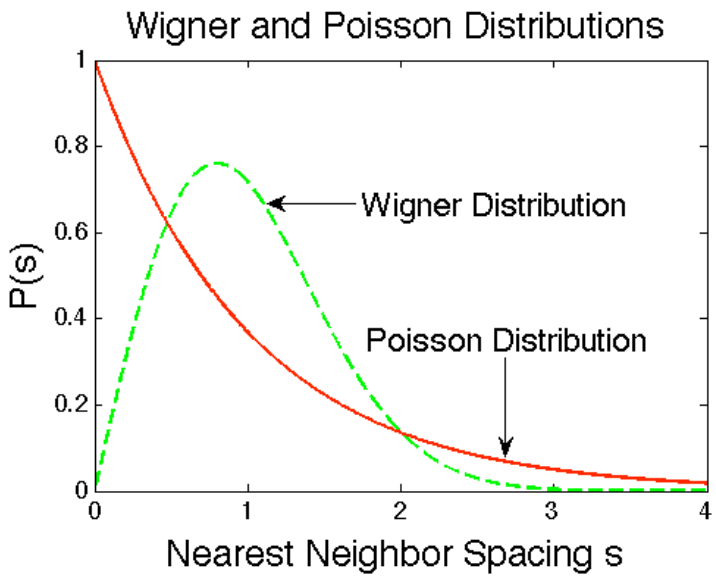

Figure 2.1: The Wigner and Poisson probability distributions.

able to approximate the critical disorder by identifying at which level of disorder they all intersect each other.

Chapter 3

Inverse Participation Ratio and Localization

To explore the localization transition on glued trees, we begin by verifying that the transition is qualitatively similar on both glued trees and branched trees by comparing the corresponding IPR plots.

In order to make these IPR plots, we must determine the IPR corresponding to the eigenvectors for each level of disorder, and average the IPR over many instances of the random Hamiltonian. Specifically, for each level of disorder we generate a random Hamiltonian corresponding to the graph, then calculate its eigenvalues and eigenvectors. From the eigenvectors we can then calculate the corresponding inverse participation ratio. We then bin the inverse participation ratio by the corresponding eigenvalues, averaging within each bin. Finally, we average the bins over many instances of the random Hamiltonian to get the plots in this section.

We now look at how the IPR behaves for each type of graph we have introduced in order to determine where the onset of localization occurs for that graph. Because of the apparent deficiencies of the simple trees in allowing many nodes that don't have the local structure of the Cayley tree, the IPR plots for the simple trees should be viewed somewhat skeptically.

For the simple branched tree, we see that the Figure 3.1(a) behaves roughly as expected, and corresponds pretty well with the prediction by Abou-Chacra et al. [ACT] for an infinite branched tree, which suggests that the critical disorder is roughly 17, which would then corresponds to an IPR of approximately 0.7. However, this IPR plot exhibits certain features that don't vary smoothly. Foremost among these are the "horns" near the origin that exhibit a high IPR at even very low levels of disorder. There also appears to be a sudden transition to higher IPR at energies approximately equal to the disorder. These features that don't vary smoothly call into question the validity of our averaging, which implicitly assumes that within each energy bin the IPR should be nearly constant. Moreover, there are surprisingly few areas where the IPR is truly low (deep blue), as we'd expect the extended states to involve at least

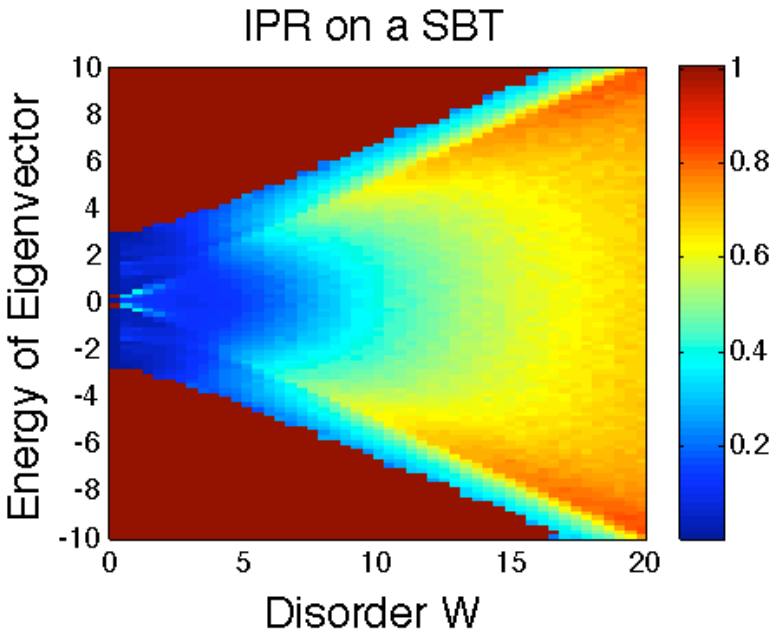

(a)

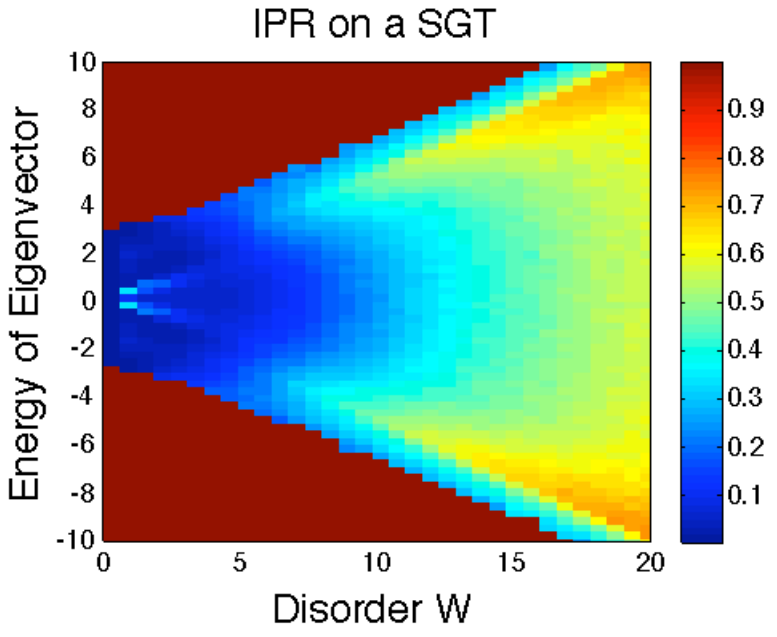

(b)

Figure 3.1: **(a):** This has anomalous features near the origin, and the IPR tends to increase faster than expected. **(b):** The simple glued tree exhibits similar behavior, though the IPR increases more slowly.

several hundred sites for a tree with roughly $1,000$ nodes, and thus have a negligible IPR.

For the simple glued tree, the behavior in Figure 3.1(b) looks quite similar to that of the simple branched tree, though in this case the disorder and energy scales needed to be extended a little to reveal areas similar to that for the branched tree, which suggests that glued trees have a greater critical disorder than branched trees — roughly 24 if we use an IPR of 0.7 to determine the mobility edge.

However, the modified branched tree exhibits strikingly different behavior than the simple branched tree, as seen in Figure 3.3(a). The horns of the previous graph have vanished, and we are left with an ocean of deep blue at low disorders, which transitions gradually to the hotter colors. This more gradual transition now seems to suggest that the critical disorder corresponds to an IPR around 1/3, rather than the .7 suggested from the simple branched tree. As this tree corresponds more closely with the Cayley tree [SB], we will use an IPR of roughly 1/3 to determine the critical disorder for the modified glued tree.

The IPR plot for the modified glued tree in Figure 3.3(b) looks remarkably similar to that for the modified branched tree. If we look for the transition to an IPR of 1/3, we find that it occurs just above a critical disorder of 16, so it appears that the critical disorder of the modified glued tree is comparable to that of the modified branched tree.

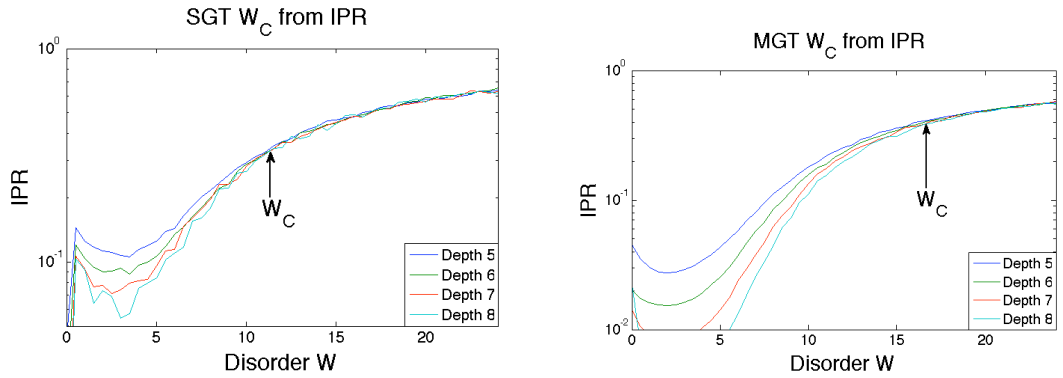

(a) (b)

Figure 3.2: Since the localization transition should be depth-independent, we can determine W_C by seeing the convergence of the IPR of a state in the band center at different depths. **(a):** The curves for a simple glued tree seem to coalesce for $W_C \approx 12$. **(b):** On the other hand, the curves for a modified glued tree seem to converge for $W_C \approx 16$, roughly in line with analytical predictions for the Cayley tree.

However, as we noted in section 2.2, we can get a more accurate idea of the critical disorder by plotting the IPR of a eigenvector at the band center for multiple tree depths and see where the resulting curves first merge. Doing this, we find that

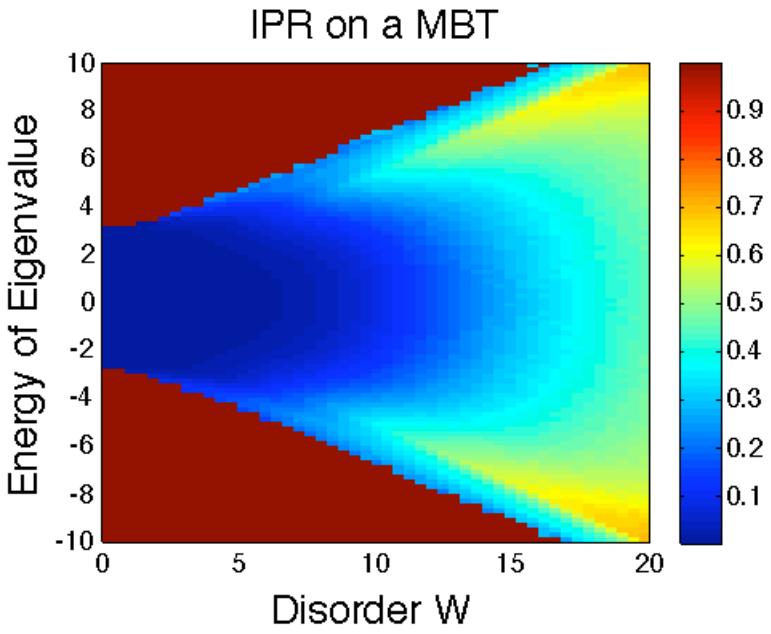

(a)

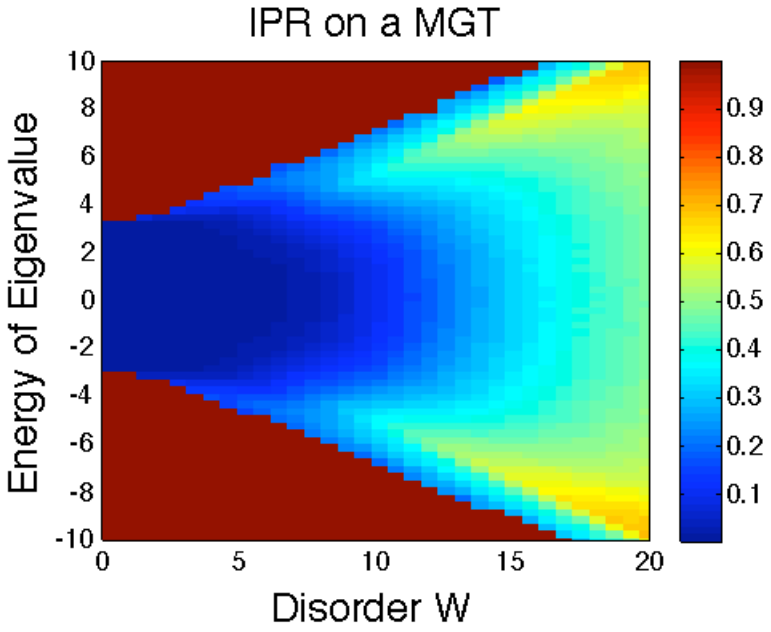

(b)

Figure 3.3: **(a):** This has a much larger region of very low IPR, as would be expected inside the mobility edge. The IPR also tends to increase more slowly. **(b):** The IPR for modified glued trees behaves quite similarly.

the behavior of the simple trees is more in line with our expectations, and follow the analytical predictions quite closely. Since the glued trees are of particular interest, we have isolated their results in Figures 3.2(a) and 3.2(b). For the simple glued trees, we see that this method predicts $W_C \approx 12$, whereas for the modified glued trees it predicts $W_C \approx 16$. However, determining when and where the curves have converged sufficiently is quite subjective, so this method permits large error terms.

Chapter 4

Nearest Neighbor Spacing Distributions and Localization

We can also look at other quantities to analyze the localization transition. Following the analysis of [SB] we look at the normalized level spacings and see what can be inferred about the transition from these level spacings.

To numerically calculate the nearest neighbor spacing distribution, we simply generate an instance of the Hamiltonian, solve the eigenvalue equation to obtain and sort the eigenvalues, then look at the spacing between adjacent eigenvalues. We then normalize the distribution to have mean 1 by setting

$$s = \frac{E_{i+1} - E_i}{\langle E_{i+1} - E_i \rangle}. \tag{4.1}$$

As was discussed during the section 2.3 on Random Matrix Theory, we expect that as the disorder is increased we will observe a transition from the Wigner surmise distribution given by

$$P_W(s) = \frac{\pi}{2} s \exp\left(-\frac{\pi}{4} s^2\right) \tag{4.2}$$

to the standard Poisson distribution $P_P(s) = e^{-s}$.

Moreover, since all of the distributions should intersect near $s = 2$, we can derive another quantity that measures how localized the state is by looking at the mass of the probability distribution beyond $s = 2$, setting

$$\gamma = \frac{\int_2^\infty P(s) \ - \ \int_2^\infty P_W(s)}{\int_2^\infty P_P(s) \ - \ \int_2^\infty P_W(s)}. \tag{4.3}$$

By tracking how γ behaves as the disorder increases we can quantify the transition from Wigner-like behavior to Poisson-like behavior, with Wigner-like behavior meaning that $\gamma \approx 0$, whereas Poisson-like behavior means that $\gamma \approx 1$, so higher γ correlates with a more localized state. Moreover, at the critical disorder the level-spacing distribution $P(s)$ (and hence γ) should be independent of the size of the system [SB], so the critical disorder is identified with the intersection of these lines.

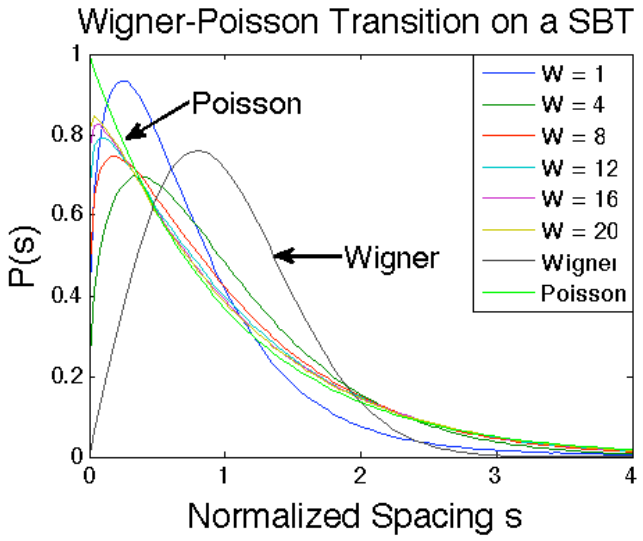

(a)

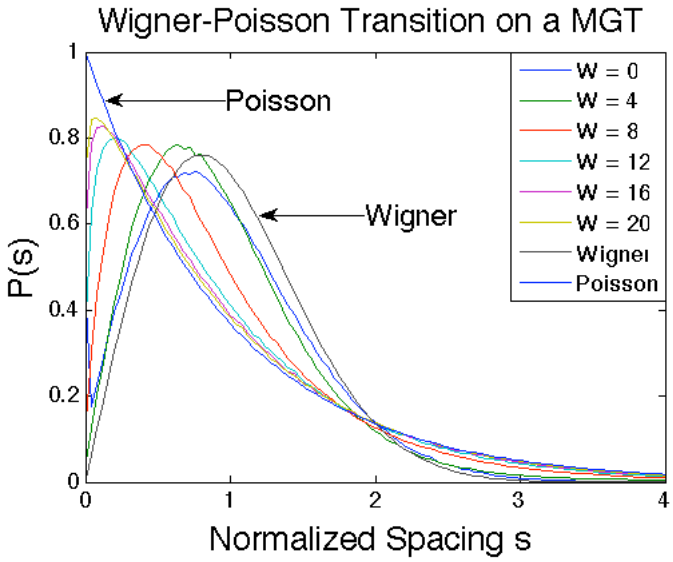

(b)

Figure 4.1: **(a):** The nearest neighbor spacing distribution is plotted for a SBT for multiple levels of disorder. Unexpectedly, at low disorder the distribution does not conform to the Wigner distribution, but is instead quite different—the plot begins at $W = 1$ since at lower levels of disorder it is too tightly peaked around $s = 0$! As the disorder increases, the distribution does appear to tend towards the Poisson distribution, as expected. **(b):** A similar plot for a MGT. This plot exhibits a smooth transition from a nearly Wigner distribution at low disorder to a Poisson distribution at higher disorder. Deviations from the Wigner distribution at low disorder are likely due to the finite size of the graph.

Thus, for a given level of disorder we will generate a random Hamiltonian and calculate the nearest neighbor spacing distribution for that Hamiltonian. We will then average over many instances of Hamiltonians, and use this to approximate the nearest neighbor spacing distribution, which we can plot at this point. From the nearest neighbor spacing distribution, we can then approximate γ. This process will be repeated for multiple levels of disorder for each tree depth, and then for multiple tree depths for each type of tree. We will then make plots of γ for multiple depths of each type of tree and use these plots to approximate the critical disorder.

Applying this method of analysis to each type of tree we again see that the simple trees exhibit anomalous behavior, hence we will subsequently ignore them for the purposes of predicting the critical value of the localization transition and for the remainder of this paper.

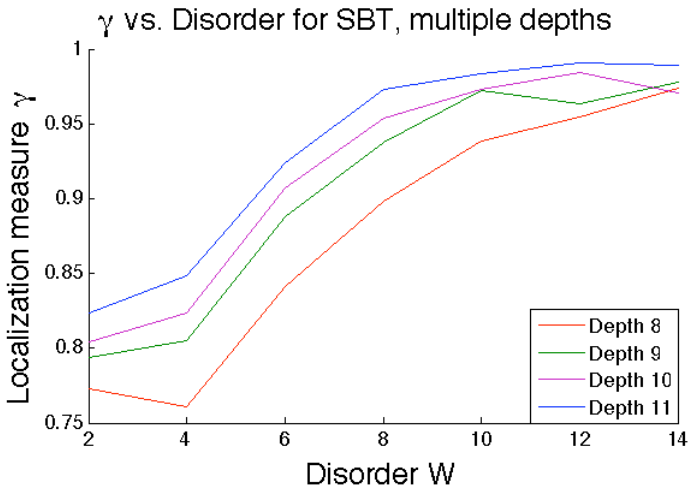

Figure 4.2: As one can see from this plot, there is no point where the measure γ is the same at each depth, and thus there is no identification of the critical disorder, even though it's expected that the critical disorder is somewhere in this range. Thus, this method fails for this graph. Also, note that even at low levels of disorder that γ is already very high, rather than starting low as expected.

For the simple branched tree, we see a number of surprising features in both the nearest neighbor spacing distribution in Figure 4.1(a) and in the plots of γ in Figure 4.2. At very low levels of disorder, rather than seeing a Wigner-like distribution with some repulsion between adjacent eigenvalues, we see that the distribution is almost entirely clumped around $s = 0$, which is quite strange. At moderate levels of disorder, the distributions seems to become more Wigner-like, but the tails tend to stay much closer to the Poisson distribution, rather than spreading out between the Wigner and Poisson tails as expected.

This strange behavior manifests itself more clearly when we look at how γ changes

for different tree sizes. Rather than seeing a steady increase in disorder approaching the localization transition, then a leveling out afterwards, the Gamma statistic is already quite large and still growing at even low levels of disorder. Moreover, increasing the tree size seems only to increase γ for all levels of disorder, rather than decreasing γ when W is below the critical disorder and increasing γ when W is above the critical disorder. The lack of this behavior then leads to a lack of intersections between the curves for γ of trees of different depths.

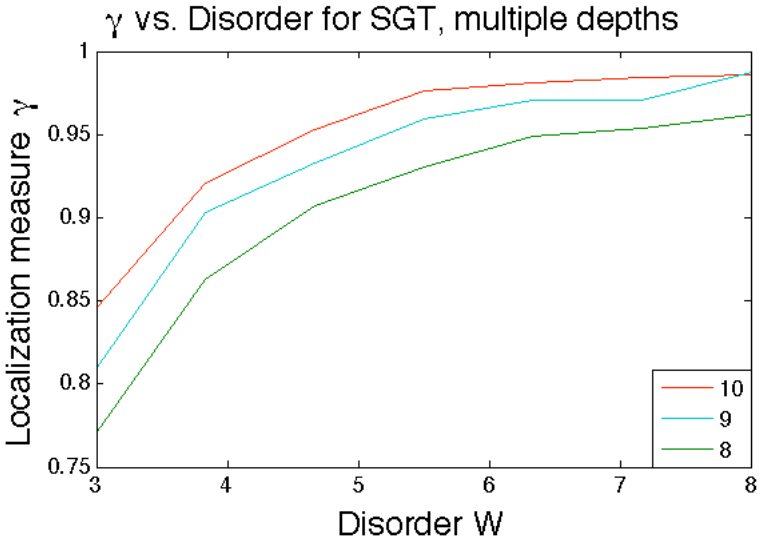

Figure 4.3: This plot is rather similar to that of the SBT plot. Even in the expected range of the localization transition, there is no indication of a universal crossover point in the curves.

Similarly, the simple glued tree exhibits behavior almost identical to that of the simple branched tree. A plot of its IPR is shown in Figure 4.3. Again, we see that the disorder starts out high, and increasing the depth of the tree only appears to increase γ for all levels of disorder, leading to no intersections between the curves. Thus, in both of these simple cases, we see no clear scale free cross-over from the Wigner distribution to the Poisson distribution, and this method fails.

If we now take a modified branched tree, our results hew much closer to those in [SB]. In the nearest neighbor spacing distribution in Figure 4.1(b) we see a nice, smooth transition from the Wigner distribution to the Poisson distribution as the disorder is increased, with the tails moving smoothly between the two distributions as well. Moreover, when we plot gamma versus the disorder for multiple tree sizes, we do see a universal intersection point occurring near $W = 12$, in rough agreement with the result in [SB], so this procedure now succeeds in identifying the critical disorder.

Finally, for the modified glued tree, the system of greatest interest, we see the same qualitative behavior as for the modified branched tree. However, now the intersection

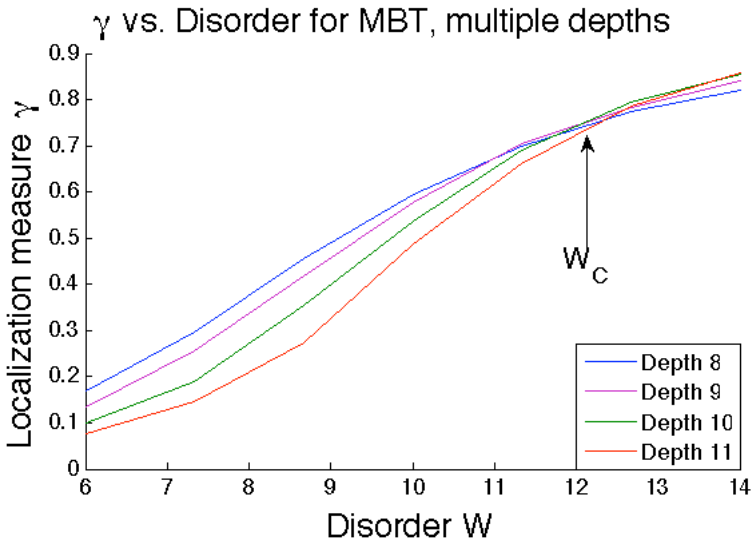

Figure 4.4: With the modifications, the γ plots now deliver the expected behavior for the MBT. Even at a moderate level of disorder of $W = 6$, the γ is quite low, then as W increases the curves converge near $W_C = 12$.

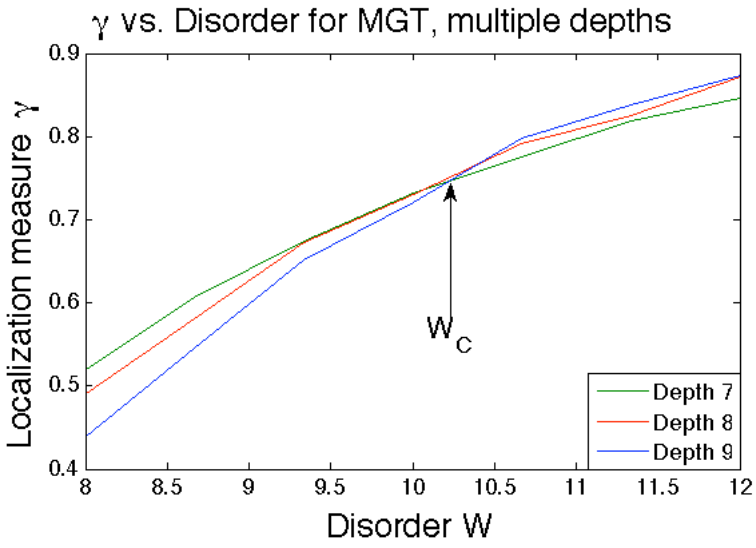

Figure 4.5: Again, the modifications to the glued tree yield the expected behavior, with a universal intersection point occurring around $W_C = 10.25$.

of the curves,and thus the critical disorder, appears to occur between $W = 10$ and $W = 10.5$, which corroborates our observation in the IPR plots that the critical disorder for the modified glued tree is less than that for the modified branched tree.

While the calculated values for the critical disorder appear to be consistent when considering either just the IPR critical disorder of the γ-based critical disorder, there is a clear discrepancy between the values across each for both modified trees. Of course, there are also significant differences between the graphs. For zero disorder, there are a large number of degenerate states at the center of the simple glued tree [Khoo], which may bias the system away from the Wigner surmise distribution at low levels of disorder. This may explain why the γ statistic fails to work for these graphs, as well as the fact that the localization transition occurs for smaller values of W on the simple trees.

Chapter 5

Transmission Coefficients of the Modified Glued Tree

In this section we analyze the localization transition by investigating the behavior of the transmission coefficients of these graphs placed on a line. To begin, we'll extensively analyze a simple case to develop our methods, then move on to larger structures more like the systems of interest.

5.1 Line With a Split

We'll first consider the transmission on a line with a split in the middle seen in Figure 5.1, with our analysis following that of [CCF+]. Our Hamiltonian is just the adjacency matrix, along with on-site disorder ε_1 and ε_2 for the two sites at the split, indexed $0^{(1)}$ and $0^{(2)}$ respectively.

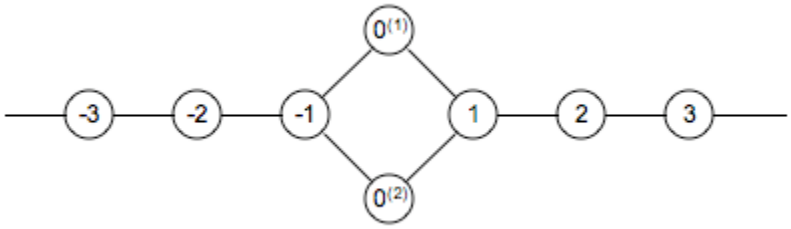

Figure 5.1: A simple graph consisting of an ingoing line (negative indices) and an outgoing line (positive indices), with a split in the middle. The central nodes have indices $0^{(1)}$ and $0^{(2)}$.

We then consider the wavefunction determined by

$$\langle j|\psi\rangle = \begin{cases} e^{ipj} + \mathcal{R}e^{-ipj} & j < 0 \\ \psi_0^{(1)} & j = 0^{(1)} \\ \psi_0^{(2)} & j = 0^{(2)} \\ \mathcal{T}e^{ipj} & j > 0 \end{cases} \tag{5.1}$$

and require that it be an eigenfunction of the Hamiltonian. Thus, we set $\mathcal{H}|\psi\rangle = E_p|\psi\rangle$, and to make it more tractable, we take the inner product with the site j on both sides, so we have

$$\langle j|\mathcal{H}|\psi\rangle = E_p\langle j|\psi\rangle, \tag{5.2}$$

which then leads to six separate equations: two away from the split, and one for each site on or adjacent to the split.

We first consider the two equations away from the split:

$$\begin{aligned} \left(\mathcal{T}e^{ip(j+1)} + \mathcal{T}e^{ip(j-1)}\right) &= E_p\mathcal{T}e^{ipj} \qquad j > 1 \\ \left(e^{ip(j+1)} + \mathcal{R}e^{-ip(j+1)} + e^{ip(j-1)} + \mathcal{R}e^{-ip(j-1)}\right) &= E_p\left(e^{ipj} + \mathcal{R}e^{-ipj}\right) \qquad j < -1. \end{aligned} \tag{5.3}$$

The first equation is easily solve for E_p, and we find that

$$E_p = 2\cos p, \tag{5.4}$$

as we would obtain for a line with no split. Substituting this into the second equation and trying to solve for $\mathcal{R}$ ends up yielding $0 = 0$, so we turn to the other equations.

The other four equations are given by

$$e^{-2ip} + \mathcal{R}e^{2ip} + \psi_0^{(1)} + \psi_0^{(2)} = E_p(e^{-ip} + \mathcal{R}e^{ip}) \tag{5.5}$$

$$e^{-ip} + \mathcal{R}e^{ip} + \varepsilon_1\psi_0^{(1)} + \mathcal{T}e^{ip} = E_p\psi_0^{(1)} \tag{5.6}$$

$$e^{-ip} + \mathcal{R}e^{ip} + \varepsilon_2\psi_0^{(2)} + \mathcal{T}e^{ip} = E_p\psi_0^{(2)} \tag{5.7}$$

$$\psi_0^{(1)} + \psi_0^{(2)} + \mathcal{T}e^{2ip} = E_p\mathcal{T}e^{ip}. \tag{5.8}$$

The easiest variables to solve for in terms of the others are clearly the $\psi_0^{(i)}$, which are given by

$$\psi_0^{(i)} = \frac{e^{-ip} + \mathcal{R}e^{ip} + \mathcal{T}e^{ip}}{2\cos p - \varepsilon_i} = \alpha_i(e^{-ip} + \mathcal{R}e^{ip} + \mathcal{T}e^{ip}), \tag{5.9}$$

where we have defined the new constant

$$\alpha_i = \frac{1}{2\cos p - \varepsilon_i} \tag{5.10}$$

for future use and neatness.

Substituting these into the first equation (5.6) involving $\mathcal{R}$, and gathering all of the $\mathcal{R}$ terms together, we find that

$$\mathcal{R}\left(e^{2ip} + (\alpha_1 + \alpha_2)e^{ip} - E_p e^{ip}\right) = E_p e^{-ip} - e^{-2ip} - (\alpha_1 + \alpha_2)(e^{-ip} + \mathcal{T}e^{ip}). \quad (5.11)$$

Substituting for E_p and solving for $\mathcal{R}$, this simplifies to

$$\mathcal{R} = e^{-ip}\left(\frac{1 - (\alpha_1 + \alpha_2)(e^{-ip} + \mathcal{T}e^{ip})}{\alpha_1 + \alpha_2 - e^{-ip}}\right). \quad (5.12)$$

Next, we substitute for the $\psi_0^{(i)}$ terms and then the $\mathcal{R}$ terms in the final equation (5.8) to get

$$\mathcal{T}(e^{ip}E_p - e^{2ip}) = (\alpha_1 + \alpha_2)\left(e^{-ip} + \left(\frac{1 - (\alpha_1 + \alpha_2)(e^{-ip} + \mathcal{T}e^{ip})}{\alpha_1 + \alpha_2 - e^{-ip}}\right) + \mathcal{T}e^{ip}\right). \quad (5.13)$$

This is now a simple but messy algebra problem which can be solved for $\mathcal{T}$ to find

$$\mathcal{T} = \frac{(\alpha_1 + \alpha_2)(1 - e^{-2ip})}{2(\alpha_1 + \alpha_2) - e^{-ip}}. \quad (5.14)$$

The form of this expression for $\mathcal{T}$ is pretty complicated, and the expression for $|\mathcal{T}|^2$ is only more so, so we will take our time to appreciate what we have learned about this simple system.

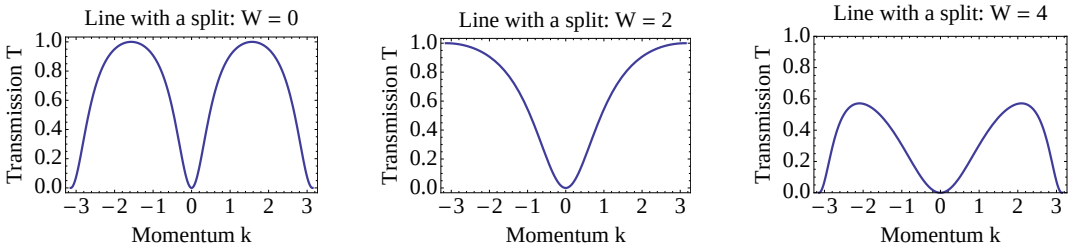

(a) (b) (c)

Figure 5.2: Plots of transmission on the line with a split in which $\varepsilon_1 = \varepsilon_2$. Full transmission is achieved for $W \in [-2, 2]$, but as W increases, the peaks of this distribution move out until they reach 0 and π **(b)**, at which point the transmission begins to decrease **(c)**.

The first thing to notice is that, unlike the example in [CCF+], this graph can achieve 100% transmission at low levels of disorder. This peak occurs at $p = \pi/2$ if there is no disorder, as in Figure 5.2(a), and can move around depending on the disorder.

Perhaps the most interesting feature is that if the on-site energy ε is the same at both sites, the graph achieves 100% transmission for some p whenever $\varepsilon \in [-2, 2]$, the extreme edge of which is seen in Figure 5.2(b), but then the transmission decays when $|\varepsilon| > 2$ as seen in Figure 5.2(c), perhaps indicating some sort of localization transition even for this simple system. Also, at $\varepsilon = -2$ the transmission peak occurs at $p = 0$ while the transmission at $p = \pi$ is 0, whereas at $\varepsilon = 2$ the transmission peak occurs at $p = \pi$ while the transmission at $p = 0$ is 0.

We can even average over uniform disorder if we take $\varepsilon_1 = \varepsilon_2 = \varepsilon$, though the general case is far more difficult. In this case, we find that

$$T = |\mathcal{T}|^2 = \frac{16 \sin^2 p}{16 \sin^2 p + 4 \cos^2 p + \varepsilon^2 + 4\varepsilon \cos p}. \tag{5.15}$$

Since the denominator is simply a quadratic in ε, we can factor it as

$$16 \sin^2 p + 4 \cos^2 p + \varepsilon^2 + 4\varepsilon \cos p = (\varepsilon + 4e^{ip})(\varepsilon + 4e^{-ip}) = (\varepsilon - \varepsilon_+)(\varepsilon - \varepsilon_-). \tag{5.16}$$

Thus, if we average $|T|^2$ over a uniformly distributed disorder of width W and center 0, we get the integral

$$\frac{16 \sin^2 p}{W} \int_{-W/2}^{W/2} \frac{1}{\varepsilon_+ - \varepsilon_-} \left(\frac{1}{\varepsilon - \varepsilon_+} - \frac{1}{\varepsilon - \varepsilon_-} \right) d\varepsilon. \tag{5.17}$$

Taking the integral of this is simple, and by combining the resulting logarithms into one term we find it equals

$$\log \left(\frac{16 - W^2/4 - 4iW \sin p}{16 - W^2/4 + 4iW \sin p} \right). \tag{5.18}$$

Since the numerator and denominator are complex conjugates of each other, all that is left is a phase $e^{-i\theta}$, where

$$\tan \theta = \frac{8W \sin p \, (16 - W^2/4)}{(16 - W^2/4)^2 - 16W^2 \sin^2 p}. \tag{5.19}$$

Thus, we find that the averaged transmission for this system is given by

$$\frac{2 \sin p}{W} \arctan \left[\frac{8W \sin p (16 - W^2/4)}{(16 - W^2/4)^2 - 16W^2 \sin^2 p} \right]. \tag{5.20}$$

5.2 Generalizing The Method to Larger Graphs

While the method introduced in the previous section is nice, in that it can eventually give an answer, it would not be very effective for larger graphs. Thus, we need a method that can quickly yield information about the transmission coefficient for

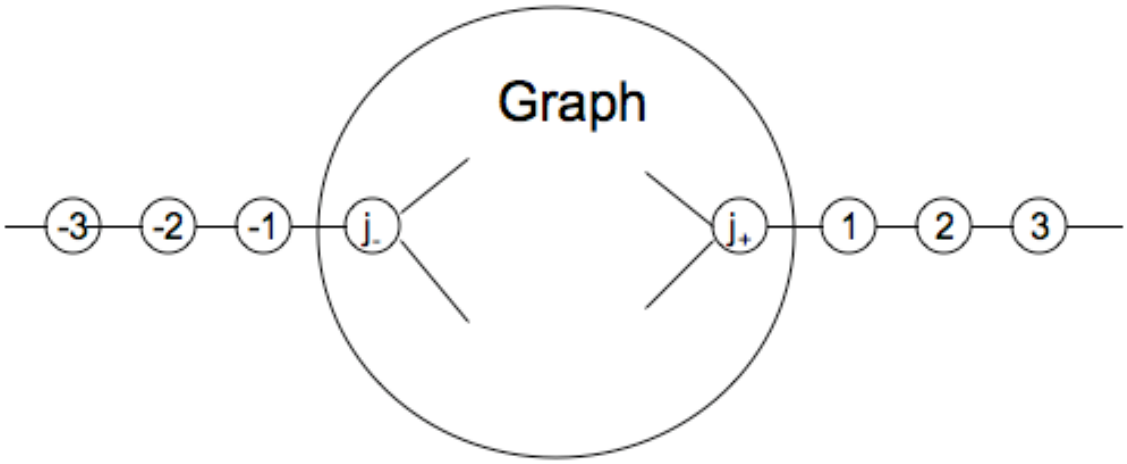

Figure 5.3: A graph with an ingoing line (negative indices) connected to it at node j_-, and an outgoing line (positive indices) connected at node j_+. The details of the rest of the graph is omitted for clarity.

larger graphs. To do this, we perform a formal matrix inversion, following Kottos in [Kot].

The basic setup can be seen in Figure 5.3, is that we have one lead going into the graph and one lead coming out of the graph, with indices as shown above — negative for the incoming lead and positive for the outgoing lead. In particular, the wave function at the leads will be $\psi^G_{j_-}$ and $\psi^G_{j_+}$ for the nodes connected to the in and out leads, respectively, and any other node in the graph will be denoted generically as ψ^G_j. The notations $(\mathcal{H}^G\psi^G)_{j_-}$ and $(\mathcal{H}^G\psi^G)_{j_+}$ will be used to denote the Hamiltonian acting on either j_- and j_+, respectively, while $(\mathcal{H}^G\psi^G)_{j\neq j_\pm}$ will be used to indicate the Hamiltonian acting on ψ^G_j individually for each j in the graph other than j_+ and j_-.

As before, we can set up equations outside of the graph by assuming that the eigenfunction consists of an incident wave, a reflected wave, and a transmitted wave on the outgoing lead. As occurred above, we find that $E_k = 2\cos k$ from the transmitted wave. We then have the four more interesting equations:

$$e^{-2ik} + \mathcal{R}e^{2ik} + \psi^G_{j_-} = 2\cos k(e^{-ik} + \mathcal{R}e^{ik}) \tag{5.21}$$

$$\mathcal{T}e^{2ik} + \psi^G_{j_+} = 2\cos k\mathcal{T}e^{ik} \tag{5.22}$$

$$e^{-ik} + \mathcal{R}e^{ik} + \left(\mathcal{H}^G\psi^G\right)_{j_-} = 2\cos k\psi^G_{j_-} \tag{5.23}$$

$$\mathcal{T}e^{ik} + \left(\mathcal{H}^G\psi^G\right)_{j_+} = 2\cos k\psi^G_{j_+}. \tag{5.24}$$

In the first two equations, we can expand out the $\cos k$ in terms of exponentials

and group like terms together, finding that

$$\psi^G_{j_-} = 1 + \mathcal{R}; \qquad \psi^G_{j_+} = \mathcal{T}. \tag{5.25}$$

This shouldn't really be of any surprise, since in the above model it was actually assumed to be true.

Substituting these results into the third equation above (5.23), we see that

$$e^{-ik} - e^{ik} + \psi^G_{j_-} e^{ik} + \left(\mathcal{H}^G \psi^G\right)_{j_-} = 2\cos k \psi^G_{j_-}, \tag{5.26}$$

which can be rearranged by grouping the terms involving wavefunctions to one side and all other terms to the other side, yielding

$$\left(\mathcal{H}^G \psi^G\right)_{j_-} - 2\cos k \psi^G_{j_-} + e^{ik}\psi^G_{j_-} = 2i \sin k, \tag{5.27}$$

while the fourth equation (5.24) becomes

$$\psi^G_{j_+} e^{ik} + \left(\mathcal{H}^G \psi^G\right)_{j_+} = 2\cos k \psi^G_{j_+}. \tag{5.28}$$

For all of the other nodes on the graph, we find that

$$\left(\mathcal{H}^G \psi^G\right)_{j \neq j_\pm} = 2\cos k \psi^G_j. \tag{5.29}$$

Thus, if we define an effective Hamiltonian

$$\tilde{\mathcal{H}}^G = \mathcal{H}^G + |j_-\rangle\langle j_-|e^{ik} + |j_+\rangle\langle j_+|e^{ik}, \tag{5.30}$$

and apply it to the entire wavefunction over the graph, since only the $|j_-\rangle$ term survives, we have

$$\left(\tilde{\mathcal{H}}^G - 2\cos k\right)\psi^G = 2i \sin k |j_-\rangle. \tag{5.31}$$

We can now invert the matrix on the left to obtain

$$\psi^G = \frac{2i \sin k}{\tilde{\mathcal{H}}^G - 2\cos k}|j_-\rangle, \tag{5.32}$$

and projecting the left along the $j+$ component thus yields $\psi^G_{j_+}$, which we've previously shown equals $\mathcal{T}$ in equation (5.25), hence we have:

$$\mathcal{T} = \psi^G_{j_+} = \langle j_+|\frac{2i \sin k}{\tilde{\mathcal{H}}^G - 2\cos k}|j_-\rangle. \tag{5.33}$$

This is our key result which allows us to efficiently calculate the transmission for a particular graph. Unsurprisingly, the transmission coefficient depends on the momentum of the incoming particle and also on the specifics of the graph, encoded in the effective Hamiltonian.

Thus, we have reduced the solution of this problem to a matrix inversion and an inner product.

In the process of performing this matrix inversion, we have made it so that the effective graph Hamiltonian $\tilde{\mathcal{H}}^G$ is no longer Hermitian, which requires some extra care. For our case, the effective Hamiltonian is a complex symmetric matrix, and to make the eigenvectors orthonormal, we need to use a modified inner product. Instead of performing a conjugate transpose to the first vector in the inner product, we must simply perform a transpose, as demonstrated in [MCF]. Henceforth, we will use this transpose vector product where we would normally use the inner product.

One of the drawbacks of this approach is that we no longer have an analytic approach to the problem. However, this disadvantage is countered by the fact that we can now see not only what the transmission will be for larger graphs, but how the transmission might scale with the depth of the graph. The results of Khoo suggest that the expected behavior for one dimensional systems is for a exponential decay in the hitting probability as the depth of the graph increases due to decay from the column space [Khoo].

5.3 Applying the Matrix Inversion to the MGT Graph

We now apply the method developed in the previous section to the MGT graphs. First, we make an analysis of the graph with zero disorder, and then we perform the analysis of the graph with diagonal disorder.

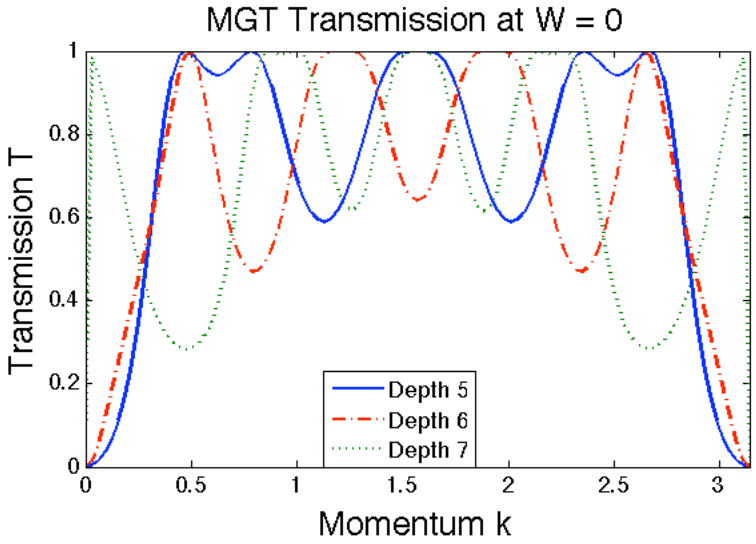

Figure 5.4: Transmission plots for MGT graphs of depths $5, 6$, and 7 as a function of the momentum k.

5.3.1 MGT with no Disorder

If there is no disorder on the MGT, then we can reduce it using the column space formalism developed in section 2.1. In this case, the only thing there is to plot is how the transmission depends on the momentum k of the incoming particle for different depths of the graph. The results are shown in Figure 5.4.

Firstly, we note that these plots are symmetric around $k = \pi/2$, as expected. Moreover, there are various resonances at different momenta depending on the size of the graph. In particular, it appears that graphs of odd depth have a local maximum at $k = \pi/2$ where $T = 1$, whereas graphs of even depth appear to have a local minimum there at approximately $T = 2/3$.

5.3.2 MGT with Diagonal Disorder

With disorder, we now make two different kinds of plots to more fully characterize the transmission: one of its dependence on the depth of the tree at the center of the energy band, and another of its dependence on both the momentum k and the disorder W.

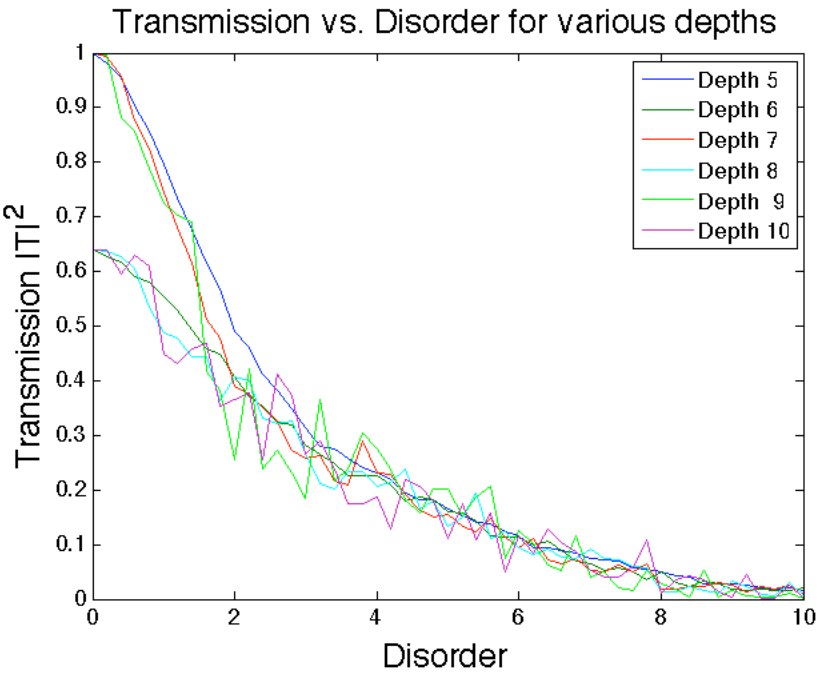

Figure 5.5: A plot of transmission at $k = \pi/2$ vs. disorder for MGT graphs of various depths. As with the zero disorder plots, we see that graphs of odd depths have higher transmission at $W = 0$. As the disorder increases the transmission appears to become depth-independent.

For the first kind we plot near the center of the band (that is, for momenta near

$\pi/2$), the transmission coefficients for trees of various depths, as seen in Figure 5.5. Specifically, we plotted the transmission at the band center for depths $5, 6, 7, 8, 9$, and 10 to see how the transmission varied with both the size of the graph and disorder.

As we have seen with the zero disorder plot in Figure 5.4, we see that at $k = \pi/2$ graphs of odd depth have $T = 1$, whereas graphs of even depth have $T \approx 0.65$ due to resonances in the transmission, similar to those with a Fabry-Perot interferometer.

For the second kind of plot, we take a given tree of depth d, then we iterate over the momentum of the incoming particle and disorder of the graph, calculate the transmission $T = |\mathcal{T}|^2$ in each case, then average over multiple instances of the graph and thus the random Hamiltonian. In doing so, we get an overview of how the transmission varies for each energy as the disorder is increased.

For our plot at $d = 5$, seen in Figure 5.6(a),we find that, as one might expect, there is little transmission for momenta near 0 and π, where the particle won't be moving quickly. In addition, the plot appears to be symmetric around $\pi/2$. However, what differences there are for low levels of disorder are soon washed away and the transmission is pretty similar for all momenta sufficiently far away from 0 or π. The plot at $d = 6$ is largely similar, but the points of maximal transition at low disorder are somewhat different because of the different resonances of the system. However, these differences are largely washed away with increasing disorder.

The most interesting and surprising feature of this pair of plots is that, although the higher depth graphs do initially appear to have somewhat greater decay in transmission, once the disorder increases beyond $W = 5$ or so the differences in the transmission coefficients diminish, and more or less appears to vanish entirely! While puzzling, this feature seems to be promising for the prospects of implementing this quantum walk on a large tree and still being able to get a speedup over the classical algorithms.

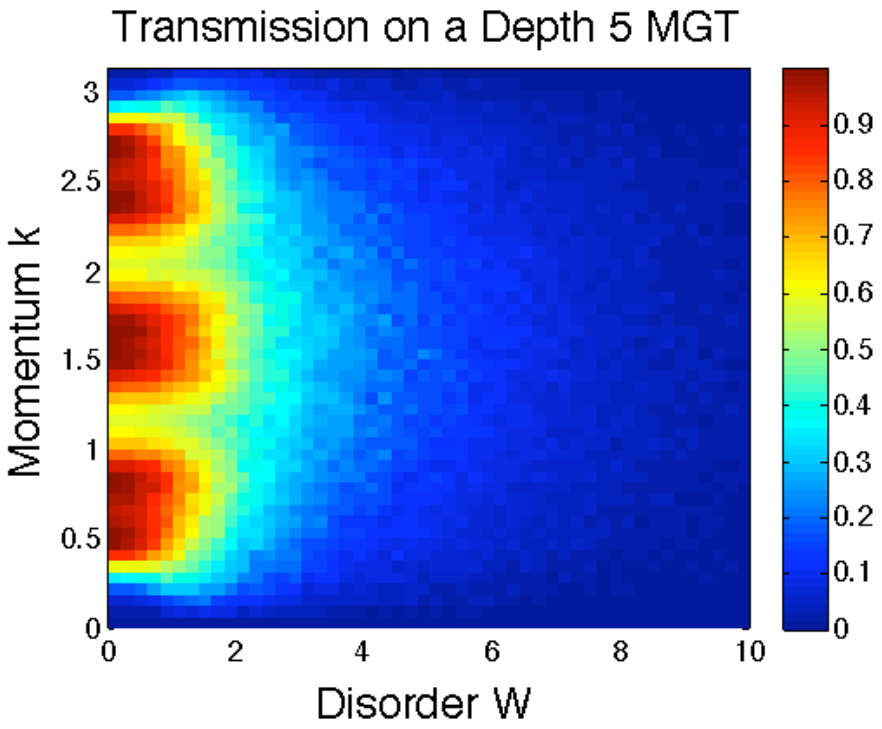
Transmission on a Depth 5 MGT
Momentum k
Disorder W
0
0.5
1
1.5
2
2.5
3
0
2
4
6
8
10
0
0.1
0.2
0.3
0.4
0.5
0.6
0.7
0.8
0.9

(a)

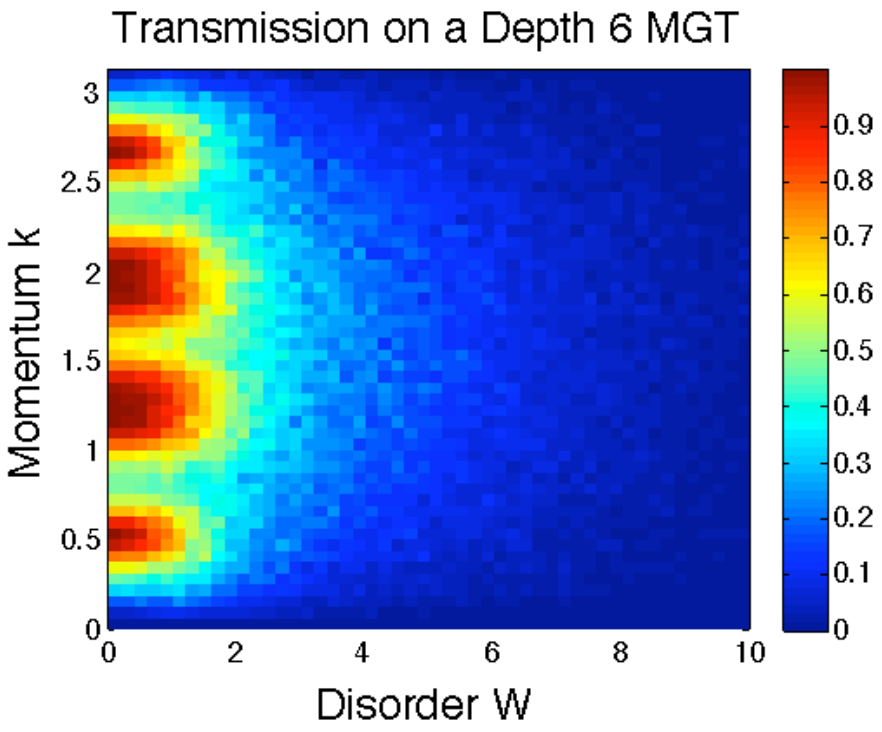
Transmission on a Depth 6 MGT
Momentum k
Disorder W
0
0.5
1
1.5
2
2.5
3
0
2
4
6
8
10
0
0.1
0.2
0.3
0.4
0.5
0.6
0.7
0.8
0.9

(b)

Figure 5.6

Chapter 6

Discussion

Firstly, our results convincingly demonstrate how important it is to preserve the local structure of the Cayley tree in both the branched trees and the glued trees. Although the Cayley tree is simply the infinite limit of the simple branched tree, the response of the simple branched tree to disorder appeared to be markedly different from that of the Cayley tree, likely due to the large number of leaf states that only have a single edge. The simple glued tree exhibited similar behavior, so our focus turned away from the simple trees and towards the modified trees, which have no leaf nodes and preserve the local structure of the Cayley tree (that is, all vertices are of degree 3) except at the start and end nodes of the trees.

Our study of the modified trees indicated that they behave rather like the Cayley tree, though the numbers for the critical disorder don't quite match up exactly. While we didn't try to calculate the errors, our result for the critical disorder of the modified branched tree lined is consistent with the value of roughly 11.5 calculated by Sade and Berkovits [SB]. Our value for the critical disorder for the modified glued tree was actually slightly lower, at a disorder just below 10.5. However, the value calculated for the Cayley tree by Abou Chacra and Thouless [ACT] is around 17, which is significantly different from the answer calculated here.

However, that value is more in line with what is observed in the IPR plots. The IPR plot for the modified branched tree is in good agreement with the analytical results for the mobility edge, and the IPR plot for the modified glued tree in turn appears to agree with the plot for the modified branched tree, though it appears that the critical level of disorder may be slightly lower.

Thus, most, but not all, signs point to the modified glued tree behaving qualitatively like the modified branched tree, and thus the Cayley tree. Since the critical disorder in the Cayley tree is quite large relative to the connection strength, it is hopeful that a physical implementation of Childs et. al's exponential speedup can be realized.

There are many questions still left open. Foremost among these is that the critical disorder for the modified branched tree, calculated using the RMT approach, is

significantly lower than the analytic results of [ACAT], a discrepancy which was also noted but not discussed in [SB]. This discrepancy could be due to the fact that these two methods are implicitly using different measures of localization, but if there really is a transition it still seems like both should agree on the critical disorder.

Another interesting question is why the modifications to the trees change the response to disorder in the way that they do. It is not so surprising that the simple branched tree behaves quite different from the modified branched tree, since roughly half of the former's nodes are leaf nodes, whereas the latter has no leaf nodes. However, the difference between the simple glued tree and the modified glued tree is a little more mystifying. Although the nodes at the middle of the simple glued tree are only of degree 2, there seems to be no obvious reason why the modifications to these nodes would have roughly the same effect on the behavior as the modifications to the leaf nodes of the simple branched tree. It certainly is fascinating, though, that the same modification that precludes the classical walk from using the local information of the tree to expedite its search for the end node also serves to make the quantum walk on a MGT more robust to disorder than one on a comparable SGT.

One could also consider a quantum walk on other graphs, both those closely related to the modified glued tree graph and those unrelated, and see how the qualities of the quantum walk and the transport are affected by the different graph structures. An example of a closely related graphs would be trees of higher degree, and seeing how the degree of the graph affects localization, while another highly interesting graph would be hypercube graphs for a various number of dimensions.

Finally, we have considered essentially static properties of these systems: namely we have been looking at solutions to the time-independent Schrodinger equation. Time-dependent calculations have shown that probability leaks out of the column space exponentially with increasing disorder [Khoo], which indicates a quantum to classical transition since the column space is intrinsically quantum mechanical. However, we should note that these calculations were for the simple glued trees graph, which may behave differently from the modified glued tree.

It would be ideal to connect the localization methods to the time-dependent nature of the quantum walk. Further possibilities of investigation in this direction are to analyze the traversal time defined in [LM] or the Wigner delay time as in [Kot] to see how the phase of the transmission affects the propagation time. If the quantum walk eventually gets through but takes infinite time to do so then our hopes for effective quantum walk algorithms in the presence of noise may be dashed.

Bibliography

[ACAT] R. Abou-Chacra, P. W. Anderson, and D. J. Thouless, *A selfconsistent theory of localization*, J. Phys. C: Vol. 6, 1973, (1734-1752).

[ACT] R. Abou-Chacra and D. J. Thouless, *Self-consistent theory of localization: II. Localization near the band edges*, J. Phys. C: Vol. 7, 1974, (65-75).

[BFL+] M.A. Broome, A. Fedrizzi, B.P. Lanyon et al., *Discrete Single-Photon Quantum Walks with Tunable Decoherence*, Physical Review Letters **104**, 153602 (2010).

[Bose] S. Bose, *Quantum Communication through an Unmodulated Spin Chain*, Physical Review Letters **91**, 207901 (2003).

[BST] G. Biroli, G. Semerjian, and M. Tarzia, *Anderson model on Bethe lattices: density of states, localization properties, and isolated eigenvalue*, arXiv:1005.0342v1.

[CCF+] A. M. Childs, R. Cleve, E. Farhi, et al., *Exponential algorithmic speedup by quantum walk*, Proc. 35th ACM Symp. on Theory of Computing (STOC 2003), pp. 59-68.

[CFG] A. M. Childs, E. Farhi, and S. Gutmann, *An example of the difference between quantum and classical random walks*, Quantum Information Processing **1**, 35 (2002).

[Chi] A. M. Childs, *Universal computation by quantum walk*, Physical Review Letters **102**, 180501 (2009).

[DWM] M. H. Devoret, A. Wallraff, and J. M. Martinis, *Superconducting Qubits: A Short Review*, arXiv:cond-mat/0411174v1.

[FM] F. W. K. Firk and S. J. Miller, *Nuclei, Primes, and the Random Matrix Connection*, arXiv:0909.4914v1

[FGG] E. Farhi, J. Goldstone, and S. Gutmann, *A Quantum Algorithm for the Hamiltonian NAND Tree*, arXiv:quant-ph/0702144v2.

[GGC] A. Garcia-Garcia and E. Cuevas, *Dimensional dependence of the metal-insulator transition*, Physical Review B **75**, 174203 (2007).

[GMW] T. Guhr, A. Muller-Groeling, and H. A. Weidenmuller, *Random Matrix Theories in Quantum Phyiscs: Common Concepts*, Physics Reports **299** (1998), 189-425.

[HMF+] F. Helmer, M. Mariantoni, A. G. Fowler et al., *Cavity grid for scalable quantum computation with superconducting circuits*, Europhysics Letters **85**, 50007 (2009).

[Kempe] J. Kempe, *Quantum random walks: an introductory review*, Contemporary Physics **44**, no. 4 (2003), 307-327.

[KFC+] M. Karski, L. Forster, J. Choi, et al., *Quantum Walk in Position Space with Single Optically Trapped Atoms*, Science **325** (2009), 174-177.

[Khoo] T. Khoo, *Disorder, Localization, and Decay in Quantum Walks*, Williams College Report (2009).

[Klein] A. Klein, *Extended States in the Anderson Model in the Bethe Lattice*, Advances in Mathematics **133**, 163-184 (1998).

[KLMW] J.P. Keating, N. Linden, J.C.F. Matthews, and A. Winter, *Localization and its consequences for quantum walk algorithms and quantum communication*, Physics Review A **76** 012315 (2007).

[Kot] T. Kottos, *Statistics of resonances and delay times in random media: beyond random matrix theory*, J. Phys. A: Math. Gen., Vol. 38, 2005.

[Kra] V. E. Kravtsov, *Random Matrix Theory: Wigner-Dyson statistics and beyond*, arXiv:0911.0639v1

[KS] T. Khoo and F. Strauch, Private Communication.

[LM] R. Landauer and Th. Martin, *Barrier interaction time in tunneling*, Reviews of Modern Physics **66** (1994), No. 1, 217-228.

[MCF] N. Moiseyev, P. R. Certain, and F. Weinhold, *Resonance properties of complex-rotated hamiltonians*, Molecular Physics, 1978, Vol. 36, No. 6, 1613-1630.

[MD] J. D. Miller and B. Derrida, *Weak-Disorder Expansion for the Anderson Model on a Tree*, Journal of Statistical Physics Vol. 75, Nos. 3/4, 1994, pp. 357-388.

[MF] A. D. Mirlin and Y. V. Fyodorov, *Localization Transition in the Anderson Model on the Bethe Lattice: Spontaneous Symmetry Breaking and Correlation Functions*, Nuclear Physics B **366** (1991), pp. 507-532.

[MK] J. A. Mendez-Bermudez and T. Kottos, *Probing the eigenfunction fractality using Wigner delay times*, Physics Review B, Vol. 72, 2005.

[Mir] A. D. Mirlin, *Statistics of energy levels and eigenfunctions in disordered systems*, Physics Reports **326** (2000), 259-382.

[MTB] S. J. Miller and R. Takloo-Bighash, *An Invitation to Modern Number Theory*, Princeton University Press, Princeton, NJ, 2006.

[OF] A. Ossipov and Y. V. Fyodorov, *Statistics of delay times in mesoscopic systems as a manifestation of eigenfunction fluctuations*, Physical Review B, **71** (2005).

[PL] L. Sanchez-Palencia and M. Lewenstein, *Disordered quantum gases under control*, Nature Physics, **6** (2010), 87-95.

[RMKLA] P. Rebentrost, M. Mohseni, I. Kassal, S. Lloyd, and A. Aspuru-Guzik, *Environment-assisted quantum transport*, New Journal of Physics **11** (2009), 033003.

[SB] M. Sade and R. Berkovits, *Study of the Localization Transition on a Cayley-tree via Spectral Statistics*, Physical Review B, **68** (2003), 193102.

[SW] F. W. Strauch and C. J. Williams, *Theoretical analysis of perfect quantum state transfer with superconducting research*, Physical Review B **78**, 094516, (2008).

[SKHB] M. Sade, T. Kalisky, S. Havlin, and R. Berkovits, *Localization transition on complex networks via spectral statistics*, Physical Review E, **72** (2005), 066123.

[SP] K. M. Slevin and J. B. Pendry, *Electron localisation in 1D—the general case* J. Phys. C, **21** (1988) 141-149.

[VB] M. Varbanov and T. A. Brun, *Quantum scattering theory on graphs with tails*, Physical Review A, **80**, 052330 (2009).

[ZKG+] F. Zahringer, G. Kirchmair, R. Gerritsma, et al., *Realization of a Quantum Walk with One and Two Trapped Ions*, Physical Review Letters **104**, 100503.